

Accounts

Solvation Structures and Solvent Exchange Reactions of Metal Ions in Various Coordinating Solvents

Shigenobu Funahashi* **and Yasuhiro Inada†**

Laboratory of Analytical Chemistry, Graduate School of Science, Nagoya University, Chikusa-ku, Nagoya 464-8602

†Research Center for Materials Science, Nagoya University, Chikusa-ku, Nagoya 464-8602

(Received January 10, 2002)

The solvation structures and the reaction mechanisms of the solvent exchange reactions of metal ions are essential aspects of the interactions of the metal ions with the solvent molecules and information about them is necessary to understand the reactivities of the metal ions in solution. The solvation structures in various coordinating solvents were discussed on the basis of the structure parameters determined by the extended X-ray absorption fine structure technique, referring to the ionic size, ionic charge, and electronic configuration of the metal ions and the bulkiness and electron donating ability of the solvent molecules. It was shown that the deficient bulkiness of 1,1,3,3-tetramethylurea leads to a unique variation in the solvation number for a series of 3d-block metal ions and that the strong electron donating ability of propylamine reduces the solvation number. The solvent exchange mechanisms of various metal ions were discussed on the basis of the activation parameters determined by the nuclear magnetic resonance technique, and the effects of the ionic charge, ionic size, and electronic configuration of the metal ions were regularized. The kinetic results for the solvent exchange of the Ni^{2+} and Mn^{2+} ions in a series of nitriles revealed the effect of the solvent bulkiness on the variation in the mechanism. The kinetic chelate effect was pointed out on the basis of the activation parameters for the solvent exchange of the divalent first-row transition metal ions in bidentate solvents such as ethylenediamine and trimethylenediamine.

Much of chemistry pertains to and is conducted in solutions and involves ionic species. The ions interact with one another and with nonelectrolytes. The extent of these interactions and the rate of any reactions in which the ions take a part strongly depend on the nature of the solvent present, i.e., the ion–solvent interactions. These are generally sufficiently strong that the properties relevant for any further interactions or reactions become those of the solvated ion. Thus, the process of solvation of the metal ion is most essential and important to understand the physicochemical properties of the solution containing the metal ion, and a large number of investigations have been performed to clarify the solvation phenomena.

Due to the development of scattering techniques using X-rays and neutrons, structural information about solutions has become available on the pm distance scale.[1,2] A nonhomogeneous distribution of solvent molecules around the metal ion is revealed; the importance of microscopic descriptions of the solvent has been indicated, especially in the local region around the metal ion. According to the radial distribution function for the interaction between the metal ion and solvent molecules obtained by the diffraction experiments and the molecular simulations, there is no doubt that the solvent molecules form a few shells around the metal ion not only in water but also in nonaqueous solvents. Especially in the neighborhood of the metal ion, some solvent molecules aggregate to form a distinct shell. The first neighboring solvent molecules in coordinating solvents directly bind to the metal ion, and the first solvation sphere is formed by the metal ion and the first shell of the coordinating solvent molecules. The Coulombic potential of the metal ion affects the surroundings of the metal ion over a long distance range and arranges the solvent molecules around the first solvation sphere. This leads to an increased distribution probability of solvents and the second solvation sphere is formed. The radial distribution of the solvent molecules in the second solvation sphere is generally broad and the constraint is weaker than that in the first solvation sphere. Since the most significant energies are produced by the direct interaction between the metal ion and the solvent molecules in the first solvation sphere, the structure of the first solvation sphere, referred to the "solvation structure" of the metal ion, is the most crucial piece of structural information about the metal ion in solution. In this article, we will evaluate the factors which affect the solvation structure. For the properties of the solvent molecules, the steric bulkiness should be an important factor in addition to its electronic characteristics. We will review the solvation structure of the metal ions in

some bulky solvents and estimate the bulkiness of a variety of coordinating solvent molecules according to the variation in the solvation structure.

The solvent molecules in the first solvation sphere of the metal ion are dynamically exchanged with those in the second solvation sphere. The solvent exchange reaction is the most basic chemical reaction that occurs on the metal ion in solution. All complexation reactions of the metal ion are regarded as an optional exchange of the solvent molecule in the first solvation sphere with the complexing ligand, and some redox reactions of the metal ion proceed via complexation reactions with the redox pair before the actual electron transfer. The solvent exchange reaction of a solvated metal ion ($[MS_n]^{m+}$) with the solvation number of n in solvent S is expressed as Eq. 1,

$$[MS_n]^{m+} + S^* \overset{k_{ex}}{\rightleftarrows} [MS^*S_{n-1}]^{m+} + S \quad (1)$$

where S^* is the entering solvent molecule in the second solvation sphere and k_{ex} denotes the first-order rate constant of the solvent exchange reaction, defined as the reciprocal of the average interval time between two successive exchanges for any solvent molecules in the first solvation sphere. As is apparent from Eq. 1, the free energy change of the solvent exchange reaction is zero, and the activation processes of the forward and reverse direction should be the same (microscopic reversibility). The k_{ex} value is therefore the most primitive rate constant of the metal ion and is a criterion to measure the reactivity in the solvent.

The mechanistic interpretation of the solvent exchange reaction is very useful to understand the reaction profile of the metal ion. The most widely used classification of the reaction mechanism for the ligand substitution reactions has been proposed by Langford and Gray,[3] and their classification has been adopted for the solvent exchange reactions. In their model, the reaction mechanisms are classified into five categories: i.e., the associative (A) mechanism, the associative interchange (I_a) mechanism, the interchange (I) mechanism, the dissociative interchange (I_d) mechanism, and the dissociative (D) mechanism. For the solvent exchange reactions, the A mechanism is defined as the reaction taking an intermediate with the increased solvation number of the metal ion after the transition state, while the reaction of the D mechanism proceeds via an intermediate with a reduced solvation number. These two limiting mechanisms are characterized by the existence of a discernible intermediate, and the exchanging solvent molecules are not identical at the transition state. In the case of the other three mechanisms (I_a, I, and I_d), an intermediate is not assumed during the exchange process, and the association of an entering solvent and the dissociation of a leaving solvent occurred competitively. The difference is in the degree of bond making with the entering solvent and in the degree of bond breaking with the leaving solvent. When the contribution of the bond making exceeds that of the bond breaking, the reaction is classified as the I_a mechanism, while the opposite contributions result in the I_d mechanism. If these two contributions are the same, the reaction is assigned to the I mechanism. Since the entering and leaving solvent molecules are identical in the transition state for these competitive mechanisms, the difference between the mechanisms is based on the location of the two exchanging solvent molecules. As in the case of the static solvation structures, the dynamic solvent exchange behaviors of the metal ion should be influenced by the properties of both the metal ion and the solvent molecule. We will present how the reaction mechanisms are varied in response to various properties, clarified by some systematic investigations of the solvent exchange kinetics in a variety of coordinating solvents.

In this article, we will use the following abbreviations for solvents.

AN	acetonitrile
BuN	butyronitrile
iBuN	isobutyronitrile
BzN	benzonitrile
DMA	*N*,*N*-dimethylacetamide
DMF	*N*,*N*-dimethylformamide
DMPU	*N*,*N*′-dimethylpropyleneurea
26DMPY	2,6-dimethylpyridine
DMSO	dimethyl sulfoxide
EN	ethylenediamine
EtOH	ethanol
FA	formamide
HMPA	hexamethylphosphoramide
HOAc	acetic acid
MeOH	methanol
2MPY	2-methylpyridine
3MPY	3-methylpyridine
4MPY	4-methylpyridine
NM	nitromethane
PA	propylamine
PN	propiononitrile
PY	pyridine
TBP	tributyl phosphate
TEP	triethyl phosphate
TMP	trimethyl phosphate
TMU	1,1,3,3-tetramethylurea
TN	trimethylenediamine
VN	valeronitrile

1. Preparation of Solvated Metal Ion in Solution

In order to investigate the solvation structure and solvent exchange kinetics, it is very important to prepare sample solutions in which only the solvated metal ions and the counter ions exist. First of all, a suitable selection of the counter ion of each metal ion is necessary to prevent any direct coordination of the counter ion to the metal ion, since the reactivity of the metal ion is expected to be drastically changed by any coordination of the counter ion. Especially, in nonaqueous solvents, since the dielectric constant is generally small, there is a large tendency to form not only the ion pairs but also the directly bound complexes. The use of a suitable counter ion with a low coordinating ability is thus essential to avoid the complexity of solvated species. Since the coordinating ability of ClO_4^- is quite low, ClO_4^- is used as the counter ion in many experiments. The $CF_3SO_3^-$ and $CH_3C_6H_4SO_3^-$ ions are also considered to be suitable because of their low coordinating ability in comparison to F^-, Cl^-, Br^-, I^-, NO_3^-, CO_3^{2-}, SO_4^{2-}, and PO_4^{3-}, and it can be noted that the $CF_3SO_3^-$ ion is very suitable since the anhydrous triflate salts of the first-row transition metal ions are obtainable.

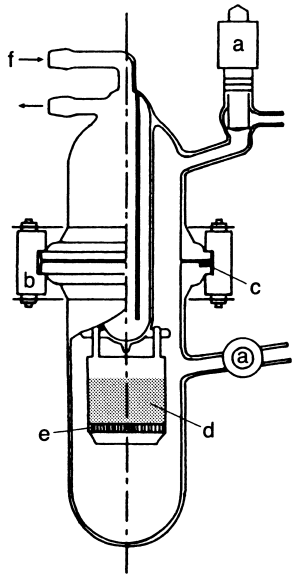

Fig. 1. Modified Soxhlet extractor. (a) greaseless vacuum valve, (b) chain clamp, (c) O-ring, (d) molecular sieves, (e) glass filter, and (f) cooling water.

Furthermore, it should be noticed that the contamination of any water present in the air must be prevented for the experiments in nonaqueous solvents. The coordinating ability of some solvents such as AN is much lower than that of water, and thus the contaminated water can bind selectively to the metal ion. In order to reduce the water content concentration, all sample solutions should be handled under a dry atmosphere not only for the preparation procedures but also for the measurement procedures. The concentration of water in solution must be confirmed to be negligible by measurements such as the Karl-Fisher method.

1.1. Use of Anhydrous Metal Salts. If anhydrous metal salts are available for the counter ion with a low coordinating ability, the contamination of water can be inhibited by just dissolving the anhydrous salts in the dried and distilled solvent. The anhydrous salts of $CF_3SO_3^-$ ($M(CF_3SO_3)_m$) for first-row transition metal ions can be prepared by drying the corresponding hydrated metal salts ($[M(H_2O)_n](CF_3SO_3)_m$), which are prepared by dissolving the suitable metal source (pure metal, metal oxide, metal carbonate, etc.) into an aqueous solution of CF_3SO_3H.

1.2. Dehydration Using Modified Soxhlet Extractor. Some anhydrous metal salts are difficult to dissolve in nonaqueous solvents or are highly hydroscopic. In such cases, it is very useful to use the modified Soxhlet extractor (Fig. 1) to remove water contained in sample solutions.[4] The hydrated metal salts are dissolved in solvent, and the solution is refluxed through activated 4Å molecular sieves in the extractor, leading to the selective trapping of the contained water. Even if the boiling point of the solvent is lower than that of water, the containing water can be removed by their azeotrope.

2. Solvation Structures of Metal Ions

The solvation structures of metal ions are most essential for examining and understanding the reactivity of the metal ions in solution. Here, some characteristics observed in the solvation structures and their interpretations are described on the basis of the available structure parameters.

2.1. Determination of Structure Parameters by EXAFS Technique. An oscillatory modulation of absorbance is observed in the X-ray absorption spectrum of the target metal ion at the higher energy side of the absorption edge.[5] This oscillation is called the extended X-ray absorption fine structure (EXAFS) and is generated by the scattering of the outgoing photoelectron wave due to the surrounding atoms around the metal ion. Thus, information about the solvation number and the bond length around the metal ion is included in the EXAFS spectrum and such structural parameters can be directly determined. Although similar information can be obtained by other techniques, such as X-ray diffraction and neutron diffraction,[1,2,6] the EXAFS technique has some characteristic advantages. One is the high selectivity. Since the energy of the X-ray absorption edge is quite different for each metal ion, structural information for the target metal ion only can be extracted. Furthermore, since the scattering of a photoelectron wave around the metal ion is restricted to a few times, the long-range interaction from the metal ion becomes a minor contribution to the EXAFS spectrum, and thus the local structure around the metal ion can be determined by the EXAFS technique. This characteristic is in marked contrast to the X-ray and neutron diffraction techniques, in which all interatomic interactions are included in the observed data. In order to obtain the solvation structure of metal ions, the EXAFS technique is thus very useful. The second characteristic is the applicability for dilute solutions. The simplest method to obtain the EXAFS spectrum is to simultaneously measure the incident and the transmitted X-ray intensities. In this case, the lowest concentration of the metal ion is limited to about 0.1 mol dm^{-3} for the 3d-block metal ions. By measuring the fluorescent X-ray intensity emitted from the sample solution instead of the transmitted X-ray intensity, the sensitivity of the EXAFS spectroscopy becomes much higher and the limitation of the sample concentrations can be reduced to the order of 10^{-4} mol dm^{-3}. On the other hand, an extremely high concentration of the metal ion is required for the X-ray and neutron diffraction techniques. In such highly concentrated solutions, the number of solvent molecules in the sample solution is sometimes not enough to fully solvate both the metal and the counter ions. Moreover, the coexisting counter ions may affect the local structure around the metal ion due to the electrostatic interaction between the counter ion and the coordinating solvent molecule.

The X-ray absorbance ($\mu_{obs,t}$) in the transmission mode is defined as $\ln(I_0/I)$, where I_0 and I denote the incident and transmitted X-ray intensities, respectively. The $\mu_{obs,t}$ value is composed of the background absorbance (μ_b), the smooth absorbance (μ_0) of the target X-ray absorbing atom without any scattering atoms around it, and the EXAFS component (μ_E) caused by the scatterers of the ejected photoelectron wave.

$$\mu_{obs,t} = \mu_b + \mu_0 + \mu_E \quad (2)$$

The X-ray energy dependence of μ_b is expressed by the Victoreen equation,[7] since μ_b mainly comes from the absorption due to the sample medium, the air in the X-ray path, the window material of the sample cell, and the detector used for the I_0

measurement. The μ_b values in the X-ray energy region higher than the absorption edge are thus estimated by the extrapolation of the X-ray absorbance in the X-ray energy region lower than the absorption edge according to the Victoreen equation. In the case of the fluorescent EXAFS measurements for dilute solutions with a sufficient sample width, the ratio (I_f/I_0) of the observed fluorescent X-ray intensity (I_f) relative to I_0 is proportional to the absorption coefficient ($\mu_{obs,f}$) of the target metal ion. The $\mu_{obs,f}$ value then corresponds to $\mu_0 + \mu_E$ in Eq. 2.

The μ_0 value is generally estimated by fitting the cubic spline function or the polynomial function to the $\mu_0 + \mu_E$ values in the X-ray energy region higher than the absorption edge. The EXAFS oscillation function ($\chi_{obs}(k)$) is then obtained by the normalization of the extracted μ_E values using Eq. 3 and the conversion of the X-ray energy to the wave number (k) of the photoelectron using Eq. 4,

$$\chi_{obs}(k) = \frac{\mu_{obs} - \mu_b - \mu_0}{\mu'_0} \quad (3)$$

$$k = \frac{2\pi\sqrt{2m(E-E_0)}}{h} \quad (4)$$

where μ'_0 is the scaled absorbance of μ_0 obtained by referring to the McMaster coefficient,[8] m is the electron mass, E_0 is the X-ray energy at the absorption edge, and h is the Plank constant. The $\chi_{obs}(k)$ values are then converted to the r-space function ($G(r)$) by the Fourier transformation,

$$G(r) = \frac{1}{\sqrt{2\pi}}\int_{k_{min}}^{k_{max}} k^3\chi_{obs}(k)W(k)\exp(-2ikr)dk \quad (5)$$

where k_{max} and k_{min} are the maximum and minimum k values, respectively, and $W(k)$ is the Hanning type window function[9] introduced to reduce the truncation error of the Fourier transformation.

On the other hand, according to the scattering theory under the assumption of dipolar excitation of an inner-shell electron and with the adoption of the muffin-tin potential for the scattering atoms, the EXAFS oscillation function is derived as Eq. 6:[10]

$$\chi_{cal}(k) = \sum_j {S_0}^2 n_j \frac{F_j(k)}{kr_j^2}\sin(2r_jk + \delta_j(k)) \exp\left(-2k^2{\sigma_j}^2 - \frac{2r_j}{\lambda_j(k)}\right) \quad (6)$$

where $F_j(k)$ is the backscattering amplitude from each of the n_j scatterers at distance r_j from the X-ray absorbing atom, $\delta_j(k)$ is the central-atom phase shift, σ_j^2 is the mean square fluctuation in r_j, $\lambda_j(k)$ is the mean free path of the photoelectron, and ${S_0}^2$ is the overall amplitude reduction factor. In a traditional treatment of the EXAFS data, the values of ${S_0}^2F_j(k)$, $\delta_j(k)$, and $\lambda_j(k)$ are empirically determined for a standard compound, using its known n_j and r_j values. An aqueous solution of the metal ion is typically used as a structural standard. A more sophisticated procedure using the FEFF program permits us to theoretically calculate the $F_j(k)$, $\delta_j(k)$, and $\lambda_j(k)$ values for all possible scattering paths, including the multiple scatterings.[11] The latter is especially useful for the EXAFS data which contain considerable contributions from the multiple scatterings. The values of n_j, r_j, and σ_j^2 are then optimized by fitting Eq. 6 to the observed $\chi_{obs}(k)$ values.[12,13] This curve fitting procedure is preferably performed in the r space by the Fourier transformation of both the $\chi_{obs}(k)$ and $\chi_{cal}(k)$ values in order to reduce the overestimation of the truncation error at the Fourier transformation.

2.2. Solvation Structures of Metal Ions in Oxygen-Donating Solvents. The solvation number (n) and the M–O bond length (r) determined by the EXAFS technique are summarized in Table 1 in some coordinating solvents with the donating oxygen atom. The hydration number (the n value in water) in Table 1 is fixed in many cases, since the EXAFS spectrum in water is used as the structural standard for other solvates in nonaqueous solvents. This procedure corresponds to the estimation of the ${S_0}^2$ term in Eq. 6, and thus the difference in the n value between in water and in nonaqueous solvents reflects the structural difference in the nonaqueous solvents relative to in water. On the other hand, since the r parameter in Eq. 6 appears in a sine term, the r value can be in principle separated from the total amplitude of the EXAFS oscillation, which correlates to both the n and ${S_0}^2$ terms. The M–O bond length varies according to the number of surrounding oxygen atoms, as seen in the values of the effective ionic radii, and thus the r value determined by the EXAFS technique should also reflect the change in the solvation number.

(1) Bulkiness Effect of Solvent Molecule. As seen from Table 1, the solvation structure is largely dependent on the bulkiness of the solvent molecule. The n values of many metal ions in MeOH and EtOH are almost the same as in water,[14] and also the solvation number in DMSO is in agreement with that in water for almost all metal ions.[14–20] Furthermore, for the majority of metal ions listed in Table 1, the n values in DMF are also regarded as being the same as in water.[15–18,21] These findings indicate that the bulkiness of the DMSO and DMF molecules does not affect the solvation structure. Here, it should be pointed out that the solvation numbers of the early members (La^{3+}–Nd^{3+}) of the lanthanide series in DMF are smaller than those in water,[22] in which the hydration number changes from 9 to 8 along the series.[23] It seems to be impossible for Ln(III) (Ln: lanthanides) ions to take a 9-coordinate solvation structure in DMF due to the bulkiness of the DMF molecule.

Although the direct structural determination of solvation structures for the metal ions with much smaller ionic radii, such as Be^{2+} and Al^{3+}, is difficult using the EXAFS technique due to their lower X-ray absorption edge energy, some useful information is obtainable using the NMR technique. The ^{9}Be NMR spectra of $[Be(H_2O)_4](ClO_4)_2$ in the mixture of water, nitrile (AN or PN), and S (S = FA, DMSO, DMF, DMA, TMP, TMU, and HMPA) show a total of five resonance peaks, as shown in Fig. 2. The systematic measurements by varying the solvent composition reveal that the five ^{9}Be NMR peaks correspond to $[Be(H_2O)_4]^{2+}$, $[Be(H_2O)_3S]^{2+}$, $[Be(H_2O)_2S_2]^{2+}$, $[Be(H_2O)S_3]^{2+}$, and $[BeS_4]^{2+}$ for all S.[24] This indicates that the solvation number of Be^{2+} is 4 not only for bulky solvents such as TMU and HMPA but also for small solvents like FA, DMSO, and DMF. According to similar investigations for Al^{3+}, the solvation structures in DMF, DMA, and TMP are concluded to be 6-coordinate octahedral, while that in TMU is 4-coordinate tetrahedral.

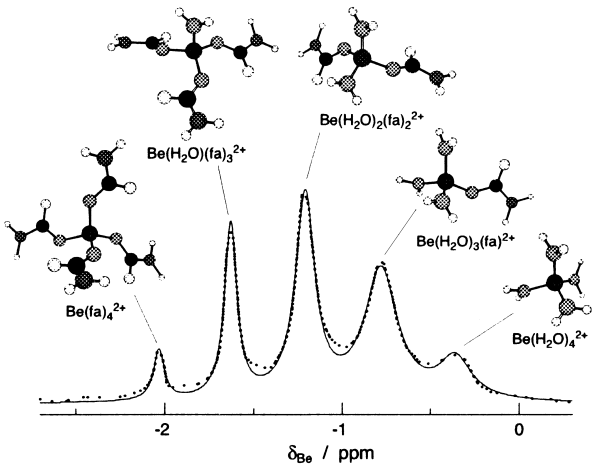

Fig. 2. ^{9}Be NMR spectrum for the propiononitrile solution containing the Be^{2+} ion (9.56×10^{-2} mol kg^{-1}), FA (0.222 mol kg^{-1}), and water (0.501 mol kg^{-1}). Dots are the observed values and a solid line represents the calculated curve obtained by the multi Lorentzian deconvolution. The reference of chemical shift (δ_{Be}) is $[Be(D_2O)_4]^{2+}$ in D_2O.

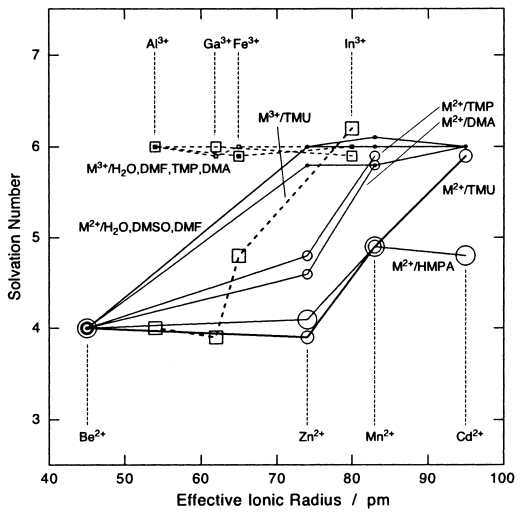

Fig. 3. The solvation number of some divalent (circles connected by solid line) and trivalent (squares connected by dashed line) metal ions in water, DMSO, DMF, TMP, DMA, TMU, and HMPA as a function of the effective ionic radius in the 6-coordinate environment. Each figure of the solvation number is given in Table 1.

In Fig. 3 are plotted the solvation numbers in water, DMSO, DMF, TMP, DMA, TMU, and HMPA of Be^{2+}, Zn^{2+}, Mn^{2+}, Cd^{2+}, Al^{3+}, Ga^{3+}, Fe^{3+}, and In^{3+} as a function of their effective ionic radii[25] in the 6-coordinate environment. Since there is no extra stabilization due to d electrons for the metal ions selected in Fig. 3, the bulkiness of the solvent molecules is expected to be focused on the solvation number variation in relation to the size of the metal ions. The solvation number in water, DMSO, and DMF given in Fig. 3 and also in MeOH and EtOH shown in Table 1 is 6 for all the metal ions except for the smallest Be^{2+} ion. However, the Zn^{2+} ion can not take the 6-coordinate solvation structure in the bulkier solvents of TMP and DMA,[14,21] in which the metal ion with the ionic radius larger than ca. 80 pm can take the 6-coordinate solvation structure. In the much bulkier solvents of TMU and HMPA, the Mn^{2+} ion with the ionic radius of 83 pm still takes a solvation number of ca. 5.[26,27] A difference between TMU and HMPA is observed for the Cd^{2+} ion, i.e., the solvation number in TMU is 6 while that in HMPA is still 5.[26,28] Similarly, the solvation number of 6 is estimated for the heavier members of the lanthanide(III) ions (Tb^{3+}–Lu^{3+}) according to the composition of the separated $[Ln(tmu)_6](ClO_4)_3$ salts and the integration of the ^{1}H NMR line of bound TMU molecules in the AN diluent.[29] The variation in the solvation number for divalent metal ions clearly corresponds to the difference in bulkiness expected from the molecular structure of the solvent molecule.

By comparing the r values for a certain metal ion with the same solvation number in the oxygen donating solvents, one will realize that the M–O bond lengths are almost constant regardless of the difference in the electron-donating and -accepting properties of the solvent molecules. This trend is in marked contrast to the case of the nitrogen donating solvents discussed below. The average M–O bond lengths (r_6, r_5, and r_4) for the 6-, 5-, and 4-coordinate solvation structures are estimated using the values in Table 1 and the values are summarized in Table 2. The difference in the M–O bond length under the different solvation number (r_6–r_5 and r_6–r_4) is almost identical to the corresponding difference in the effective ionic radius.[25] This finding indicates that the interligand repulsion between the coordinating solvent molecules is effectively relaxed under the reduced solvation number. In other words, it is considered to be not sterically crowded around the metal ion under the reduced solvation number.

(2) Effect of Ionic Charge. The change in solvation structure caused by the bulkiness of the solvent molecule is largely affected by the ionic charge of the metal ion. This is clearly observed for the solvation number in TMU. As seen in Fig. 3, the 5-coordinate solvation structure is observed for Fe^{3+} with the ionic radius of 65 pm, and the solvation number is increased to 6 for In^{3+}. The ionic radius of In^{3+} (80 pm) is intermediate between Zn^{2+} (74 pm) and Mn^{2+} (83 pm), for which the solvation numbers are reduced to 4 and 5, respectively. A similar trend is found in the case of TMP and DMA, in which the n value of Zn^{2+} is ca. 5, while the 6-coordinate solvation structures are observed for the trivalent Ga^{3+} and Fe^{3+} ions with much smaller ionic radii (62 and 65 pm, respectively). The solvation number of 6 for the trivalent metal ions with the smaller ionic radii is interpreted in terms of the stronger electrostatic interaction between the metal ion and the solvent molecules. The repulsive interaction energy between the coordinating solvent molecules and the entropy loss to form the solvated aggregate expected in the case of the larger solvation number are considered to be compensated by the larger enthalpy gain for the attractive interaction between the trivalent metal cation and the local negative charge on the coordinating oxygen atom. The solvation number of 4 for the monovalent Ag^{+} ion with much larger ionic radius (115 pm in 6-coordinate environment) is explained by the weaker attractive interaction between Ag^{+} and solvent molecules (vide infra).

(3) Effect of d Electrons. In the cases of the transition metal ions except for the Mn^{2+} and Fe^{3+} ion with d^5 configura-

Table 1. Solvation Number and Bond Length for Solvated Metal Ions in Oxygen Donating Solvents Determined by EXAFS Technique

Metal[a)]	Solvent	Conc./mol kg^{-1}	n[b)]	r/pm	Reference
Ca^{2+} (100)	H_2O	0.94	8	245	119
Cr^{3+} (61.5)	H_2O	0.1	6.1	200	120
Mn^{2+} (83.0)	H_2O	0.201	6	217	14
	MeOH	0.202	5.8	217	14
	EtOH	0.208	5.8	217	14
	DMSO	0.119	6.1	216	14
	DMF	0.192	6	216	18
		0.5	5.8	216	21
	DMA	0.5	5.8	216	21
	TMP	0.206	5.9	216	14
	TMU	0.135	4.9	209	26
	HMPA	0.020	4.9	207	27
Fe^{2+} (78.0)	H_2O	0.198	6	211	14
	MeOH	0.206	6.0	211	14
	EtOH	0.202	5.9	211	14
	DMSO	0.198	6.0	211	14
	DMF	0.191	6	210	18
		0.5	5.8	210	21
	TMP	0.511	6.0	212	14
	TMU	0.602	4.9	205	26
	HMPA	0.020	4.0	198	27
Fe^{3+} (64.5)	H_2O	0.194	6	201	121
	DMF	0.200	5.9	202	18
	DMA	0.2	5.9	200	21
	TMU	0.588	4.8	200	18
Co^{2+} (74.5)	H_2O	0.199	6	208	14
	MeOH	0.214	6.0	208	14
	EtOH	0.202	6.0	208	14
	DMSO	0.198	6.0	207	14
	DMF	0.189	6	209	18
		0.5	5.9	208	21
	DMA	0.5	5.5	207	21
	TMP	0.301	5.6	209	14
	TMU	0.505	4.1	200	26
	HMPA	0.020	3.9	195	27
Ni^{2+} (69.0)	H_2O	0.309	6	205	14
	MeOH	0.299	5.9	205	14
	EtOH	0.301	6.0	205	14
	DMSO	0.304	6.0	205	14
	DMF	0.300	6	205	18
		0.5	5.9	204	21
	DMA	0.5	5.9	205	21
Ag^{+} (115)	H_2O	0.303	4	241	16
	DMSO	0.283	3.9	238	16
	DMF	0.308	3.9	239	16
	TMP	0.273	4.0	239	16
	TMU	0.318	3.9	238	16
Cd^{2+} (95)	H_2O	0.512	6	227	26
	DMSO	0.694	6	230	17
	DMF	0.850	6	230	17
	TMU	0.851	5.9	228	26
	HMPA	0.05	4.8	223	28
In^{3+} (80.0)	H_2O	0.484	6	214	26
	DMSO	0.504	5.9	215	18
	DMF	0.729	6.0	215	18
	TMP	0.337	5.9	212	18
	TEP	0.379	5.9	211	18
	TBP	0.115	5.8	214	18
	TMU	0.448	6.2	213	26
La^{3+} (103.2)	H_2O	0.662	6[g)]	252[g)]	123
			3[g)]	264[g)]	
		0.809	9	255	22
	DMSO	0.750	8	250	123
	DMF	0.932	7.3	249	123
	DMA	0.200	6.5	247	123
	DMPU	0.080	7	244	123
Ce^{3+} (101)	H_2O	0.812	9	254	22
	DMF	0.987	8.1	247	22
	DMA	0.20	6.6	245	22
Pr^{3+} (99)	H_2O	1.397	9	250	22
	DMF	0.885	7.4	245	22
	DMA	0.193	6.9	242	22
Nd^{3+} (98.3)	H_2O	2.0	9.5	251	23
	DMF	0.913	7.4	244	22
	DMA	0.255	6.1	240	22
Sm^{3+} (95.8)	H_2O	2.0	9.3	245	23
	DMF	0.503	8.9	242	22
	DMA	0.329	8.4	237	22
Eu^{3+} (94.7)	H_2O	2.0	8.6	243	23
	DMF	0.525	7.7	239	22
	DMA	0.302	6.7	235	22
Gd^{3+} (93.8)	H_2O	2.0	7.6	241	23
	DMF	0.888	7.5	238	22
	DMA	0.303	7.2	233	22

	TMP	0.237	5.8	205	14	Tb^{3+} (92.3)	H_2O	2.0	7.5	239	23
	TMU	0.358	4.8	200	26		DMF	0.863	7.5	237	22
	HMPA	0.02	4.2	197	27		DMA	0.215	7.3	232	22
Cu^{2+} (73)	H_2O	0.208	4[c]	197[c]	14	Dy^{3+} (91.2)	H_2O	2.0	8.1	237	23
			2[d]	229[d]			DMF	0.518	7.7	236	22
	MeOH	0.202	3.8[c]	197[c]	14		DMA	0.237	7.0	230	22
	EtOH	0.201	3.9[c]	197[c]	14	Ho^{3+} (90.1)	H_2O	0.505	8	236	22
	DMSO	0.198	4.0[c]	196[c]	14		DMF	0.497	7.8	235	22
		0.50	4.0[c]	198[c]	40		DMA	0.353	6.9	229	22
	DMF	0.5	4.1[c]	196[c]	21	Er^{3+} (89.0)	H_2O	2.0	7.8	234	23
			2.0[d]	229[d]			DMF	0.597	7.2	234	22
	DMA	0.5	4.1[c]	196[c]	21		DMA	0.308	7.6	227	22
			1.8[d]	227[d]		Tm^{3+} (88.0)	H_2O	2.0	8.0	233	23
	TMP	0.388	3.9[c]	197[c]	14		DMF	0.535	7.5	232	22
			1.7[d]	214[d]			DMA	0.646	6.8	227	22
	TMU	0.489	3.9	192	26	Yb^{3+} (86.8)	H_2O	0.728	8	232	22
	HMPA	0.020	3.7	192	27		DMF	0.575	7.5	231	22
Zn^{2+} (74.0)	H_2O	0.198	6	207	14		DMA	0.298	6.3	224	22
	MeOH	0.208	6.0	208	14	Lu^{3+} (86.1)	H_2O	2.0	7.7	231	23
	EtOH	0.204	5.9	208	14		DMF	0.551	7.9	230	22
	DMSO	0.202	6.0	208	14		DMA	0.249	6.0	222	22
	DMF	0.5	5.8	208	21	Pt^{2+} (80)	H_2O	0.088	4.0	201	20
	DMA	0.5	4.6	199	21		DMSO	0.6	2.0[e]	207[e]	20
	TMP	0.344	4.8	204	14				2.0[f]	221[f]	
	TMU	0.529	3.8	195	26	Tl^{3+} (102.5)	DMSO	0.5	6	222	124
	HMPA	0.020	4.1	193	27	Bi^{3+} (103)	H_2O	0.662	8	241	19
Ga^{3+} (62.0)	H_2O	0.602	5.9	197	14		DMSO	0.40	8	241	19
	TMP	0.208	6.0	197	14		DMPU	0.10	6	232	19
	TMU	0.294	3.8	191	18	Th^{4+} (94)	H_2O	0.03	11.0	244	125
Y^{3+} (90.0)	H_2O	0.1	8.6	235	122	U^{4+} (89)	H_2O	0.05	10.7	241	125
	DMSO	0.98	8	236	15	Np^{4+} (87)	H_2O	0.005	11.2	240	126
	DMF	0.96	8	236	15	Pu^{3+} (100)	H_2O	0.020	10.2	251	126
	DMPU	0.25	6	225	15						
Pd^{2+} (86)	DMSO	2.4	2.0[e]	204[e]	20						
			2.0[f]	223[f]							
	DMF	0.5	3.8	202	18						
	TMU	0.5	3.6	202	18						

a) Each figure in parenthesis is the effective ionic radius in pm. Ref. 25. b) The integer number means that the solvation number is fixed. c) Equatorial site. d) Axial site. e) M–O interaction. f) M–S interaction. g) Assuming the 9-coordinate tricaped trigonal prismatic geometry.

Table 2. M–O Bond Lengths for 6-, 5-, and 4-Coordinate Solvation Structures

Metal	r_6[a]/pm	r_5[b]/pm	r_4[c]/pm	$r_6 - r_5$[d]	$r_6 - r_4$[d]
Mn^{2+}	217	208		9 (8)	
Fe^{2+}	211	205	198	6	13 (15)
Co^{2+}	208		195		13 (17)
Ni^{2+}	205	200	197	5 (6)	8 (14)
Zn^{2+}	208	204	194	4 (6)	14 (14)
Ga^{3+}	197		191		6 (15)
Cd^{2+}	228	223		5 (8)	

a) 6-Coordinate structure. b) 5-Coordinate structure. c) 4-Coordinate structure. d) Figure in the parenthesis denotes the difference in the effective ionic radii. Ref. 25.

tion, d elctrons on the metal ion can affect the solvation structure, i.e., the electronic stabilization responding to the geometric arragement of the coordinating solvent molecules leads to an additional contribution to the total stabilization of the solvate. A very representative example is the *n* value for the d^8 Ni^{2+} ion in TMU. According to the relationship between the ionic radius and the solvation number shown in Fig. 3, the ionic radius (69 pm in 6-coordinate environment) of Ni^{2+} is located in a region to take the 4-coordinate solvation structure. However, the *n* value was determined to be ca. 5 by the EXAFS technique. In addition, the absorption spectrum assigned to the d–d transition of Ni^{2+} in TMU clearly indicates the 5-coordinate solvation structure, and the mixture of 4- and 6-coordinate solvation structures was perfectly controverted.[26] The observed solvation number of 5 is thus interpreted to be due to an additional stabilization for the d^8 electronic configuration under the 5-coordinate structure. The unexpected larger solvation number of Ni^{2+} in TMU may come from the deficient bulkiness of TMU in comparison to HMPA, in which the solvation number of Ni^{2+} is ca. 4 (see Table 1).

A contribution of the electronic configuration to the solvation geometry is also observed in the case of Cu^{2+}. As is well known, the hydration structure of the d^9 Cu^{2+} ion is axially-elongated distorted octahedral, and this is the case in less bulky solvents such as MeOH, EtOH, DMSO, DMF, TMP, and DMA, as seen in the structure parameters given in Table 1 and as observed in the absorption spectrum; such a result is ascribed to the d–d transition in the D_{4h} symmetry.[14,30] In the much bulkier solvents of TMU and HMPA, only a single shell assigned to the Cu–O interaction was observed in the EXAFS spectrum.[26,27] Furthermore, the Cu–O bond distances (192 pm in both TMU and HMPA) are clearly different from the corresponding distance (197 pm) of the equatorial sites of the distorted octahedral structure (see Table 1). According to the d–d transition spectrum of Cu^{2+} in TMU and HMPA,[26,31] which is clearly different from the spectral pattern of the tetrahedral compounds with the CuO_4 chromophore, the four coordinating solvent molecules are suggested to be in a distorted tetrahedral arrangement in the D_{2d} symmetry.[26] Since no geometric requirements are expected to distort the arrangement from T_d, the D_{2d} distortion can be ascribed to the Jahn–Teller effect in the d^9 electronic configuration.

(4) Solvation Structure of Co^{2+} in TMU. As pointed out above, the solvation number in TMU varies from 4 to 6 in response to the ionic size, the ionic charge, and the electronic configuration of the metal ion. Here, it can be noticed that there is a unique property for the solvation structure of the divalent metal ion with the ionic radius of ca. 75 pm. According to Fig. 3, such a metal ion is expected to take the 4-coordinate tetrahedral solvation structure as in the case of Zn^{2+}, if there is no contribution from the d electron configuration. However, if the electrostatic interaction between the metal ion and the coordinating TMU molecules is much stronger, as in the case of In^{3+} with a similar ionic radius, it is possible to take the 6-coordinate octahedral structure together with an elongation of the M–O bond lengths. This means that the solvation number of the metal ion with such an ionic size is potentially variable in response to the balance between the attractive and repulsive interactions around the metal ion, and thus the solvation structure may be changeable according to the interactions in the second solvation sphere.

The most striking case is for the Co^{2+} ion with an effective ionic radius of 74.5 pm in the 6-coordinate environment. Although the *n* value of ca. 4 determined by the EXAFS technique corresponds to the ionic size of Co^{2+} as expected from Fig. 3, the observed Co–O bond length (200 pm),[26] which is 8 pm shorter than the Co–O bond length (208 pm) in the 6-coordinate solvation structure, is significantly long when considering the difference (16.5 pm) in the effective ionic radii between the 4- and 6-coordinate environments.[25] Moreover, the d–d transition spectrum of Co^{2+} in TMU has an unexpectedly small absorption coefficient and is quite different from the corresponding spectrum of the tetrahedral Co^{2+} complexes.[26] These findings strongly suggest the distortion of the CoO_4 chromophore to the D_{2d} symmetry; such a distortion is closely related to the electrostatic interaction between Co^{2+} and the TMU molecules in the second solvation sphere. The change in the absorption spectrum of Co^{2+} in the mixed solvent of TMU and NM is shown in Fig. 4.[32] The Co^{2+} ion in this system is always surrounded by four TMU molecules in the first solvation sphere, since NM is a noncoordinating solvent for Co^{2+}. Under the conditions with a low mole fraction of TMU in the bulk, the characteristic spectral pattern of the tetrahedral Co^{2+} complex is observed, while such intense absorption peaks are weakened by increasing the mole fraction of TMU and the absorption spectrum at the higher composition of TMU becomes consistent with that in neat TMU. The two-phase change in the absorbance as a function of mole fraction of TMU observed around 10 kcm^{-1} suggests that the geometric symmetry around the Co^{2+} center changes from T_d to D_{2d} via C_{3v}, as depicted in Fig. 4. This structure change occurs due to the increase in activity of TMU and is driven by the attractive interaction between Co^{2+} and one or two TMU molecules in the second solvation sphere. However, since there is no evidence to indicate such a D_{2d} distortion of the first solvation sphere for Zn^{2+} with a similar ionic radius, a more effective π interaction between the Co^{2+} ion and coordinating TMU molecules may contribute to the distortion of the first solvation sphere.

Another interesting structural variation is observed during the ligand substitution processes (Eq. 7) of $[Co(an)_6]^{2+}$ with TMU in noncoordinating NM.[33]

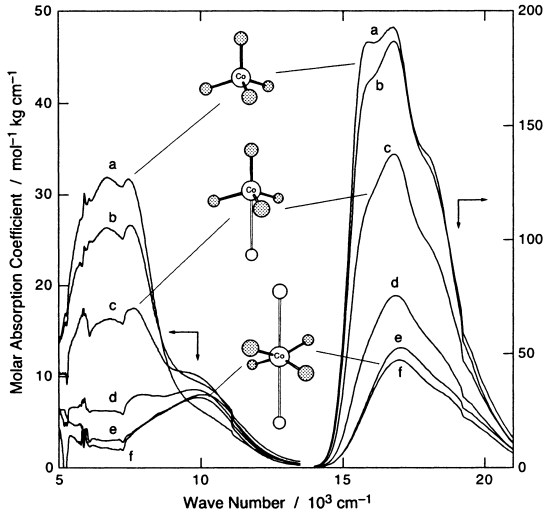

Fig. 4. Electronic absorption spectra of Co^{2+} in mixed solvent of TMU and NM. The mole fraction of TMU is 4.43 $\times 10^{-2}$ (a), 8.15 $\times 10^{-2}$ (b), 0.201 (c), 0.387 (d), 0.606 (e), and 1.00 (f). The shadowed and open circles in the inset denote the oxygen atoms of TMU in the first and second solvation sphere, respectively.

$$[Co(an)_6]^{2+} + n\text{TMU} \overset{\beta_n}{\rightleftharpoons} [Co(an)_m(tmu)_n]^{2+} + (6-m)\text{AN} \quad (n = 1-4) \tag{7}$$

The stepwise formation of $[Co(an)_m(tmu)_n]^{2+}$ was confirmed by the spectrophotometric titration. It was revealed that the ligand substitution reactions proceed as $[Co(an)_6]^{2+} \rightleftharpoons [Co(an)_5(tmu)]^{2+} \rightleftharpoons [Co(an)_3(tmu)_2]^{2+} \rightleftharpoons [Co(an)_2(tmu)_3]^{2+} \rightleftharpoons [Co(tmu)_4]^{2+}$. The 5-coordinate Co^{2+} species appear at the n values of 2 and 3, reflecting the bulkiness of the TMU molecule.

2.3. Solvation Structures of Metal Ions in Nitrogen-Donating Solvents. The solvation number and the M–N bond length determined by the EXAFS technique are summarized in Table 3 in several solvents with a donating nitrogen atom. Although nitrile solvents (AN, PN, BuN, iBuN, BzN, and VN) are largely changed in molar volume from 53 (AN) to 105 (VN) cm^3 mol^{-1}, the solvation numbers of Mn^{2+} and Ni^{2+} are always 6 in a series of nitriles,[34,35] reflecting the linear arrangement of the linear cyano group toward the metal ion.

Since the n value of Cu^+ in PY and 4MPY is 4, the bulkiness of the pyridine framework does not affect the tetrahedral solvation structure. However, the exceptional solvation number of ca. 3 for Cu^+ is seen in 2MPY and 26DMPY.[36] Such a reduced solvation number is clearly due to the interligand repulsion between the coordinating solvent molecules caused by the methyl substituents located near the donating site. It should be pointed out that the 2-coordinate structure is observed for $[Cu(26dmpy)_2]NO_3$ in the single crystal,[37] in which the planar arrangement of two pyridine frameworks is enforced by the packing requirement. Since there is no such steric restriction in solution, the 3-coordinate solvation structure may be brought about by the rotation of the pyridine plane around the Cu–N axis. Interestingly, the solvation number of Zn^{2+} in 4MPY is confirmed to be ca. 4,[38] while the 6-coordinate structure is suggested in AN.[18] This reduction of the solvation number was interpreted in terms of the bulkiness of the pyridine framework.[38] However, the reduced solvation number may also be explained in terms of the σ-donating ability of the pyridine derivative, because the solvation structure is affected by the electron-donating ability of the solvent molecule, as discussed below.

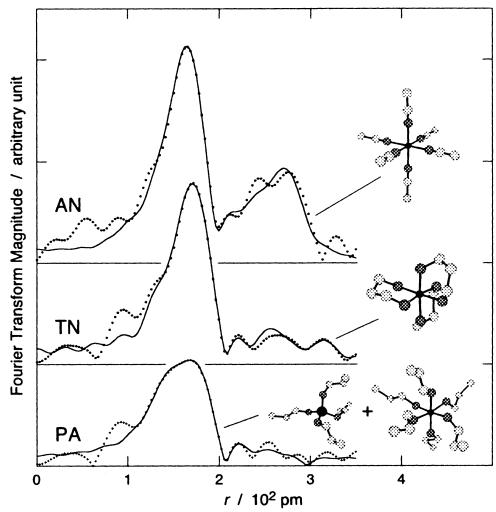

Fig. 5. Fourier transform magnitudes for Co^{2+} in AN, TN, and PA. Dotted and solid lines represent the observed and calculated values, respectively.

(1) Effect of Electron-Donating Ability. In Fig. 5, the absolute values of the Fourier transform magnitudes ($|G(r)|$) are depicted for Co^{2+} in AN, TN, and PA. The main peak in PA is remarkably distorted in comparison with those in AN and TN, indicating the mixture of two or more solvation states. The $|G(r)|$ values in PA can be well reproduced by the 7:3 mixture of the 6- and 4-coordinate solvation structures with the Co–N bond lengths (r) of 217 and 201 pm, respectively. The difference (16 pm) in r agrees with the corresponding difference in the ionic radii of Co^{2+} between the high-spin octahedral and tetrahedral geometry.[25] Furthermore, the d–d transition band of Co^{2+} in PA becomes more intense with increasing temperature, and the temperature dependence is ascribed to the change in the equilibrium constant of $[Co(pa)_6]^{2+} \rightleftharpoons [Co(pa)_4]^{2+} + 2PA$.[39] In TN, which is considered to have almost the same σ-donating ability as PA, there is no evidence of any change in the solvation number. The Co^{2+} ion is thus concluded to be octahedrally surrounded by six nitrogen atoms of three TN molecules, as supported by the slightly more intense $|G(r)|$ values in the r region of 250–350 pm in TN relative to those in PA (see Fig. 5). The EXAFS data in AN are well reproduced by the 6-coordinate octahedral structure with the linear arrangement of the cyano group to the Co^{2+} center.

The finding that the octahedral-tetrahedral (oct/tet) equilibrium of the Co^{2+} solvation is observed in PA but is not in TN indicates a difference in the entropy change, because the oct/tet conversion may accompany the release of two PA molecules in the unidentate PA and only one TN molecule in the bidentate TN. In addition, the fact that the oct/tet conversion is not observed in AN implies that the reduced solvation number of Co^{2+} in PA is caused by the strong σ-donating ability of PA,

Table 3. Solvation Number and Bond Length for Solvated Metal Ions in Nitrogen Donating Solvents Determined by EXAFS Technique

Metal[a)]	Solvent	Conc./mol kg^{-1}	n[b)]	r/pm	Reference
Mn^{2+} (83.0)	AN	0.229	6	222	34
	PN	0.217	6.0	221	34
	BuN	0.205	6.1	221	34
	iBuN	0.208	5.9	221	34
	BzN	0.100	5.7	221	34
	VN	0.200	6.1	220	34
	4MPY	0.1	5.8	225	38
	3MPY	0.1	5.7	224	38
	PA	0.326	5.9	227	118
	TN	0.272	6.1	228	118
Fe^{2+} (78.0)	AN	0.201	6	214	18
	PA	0.298	6.2	222	118
	TN	0.287	5.7	222	118
Co^{2+} (74.5)	AN	0.198	6	211	18
	4MPY	0.1	5.4	216	38
	3MPY	0.1	5.2	214	38
	PA	0.311	6[c)]	217[c)]	39
			4[c)]	201[c)]	39
	TN	0.322	6.1	217	39
Ni^{2+} (69.0)	AN	0.350	6	207	35
	PN	0.380	5.9	207	35
	BuN	0.422	6.0	207	35
	iBuN	0.383	6.0	207	35
	BzN	0.228	6.0	207	35
	VN	0.424	6.0	207	35
	4MPY	0.1	5.4	211	38
	3MPY	0.1	5.6	210	38
	EN	0.658	5.9	212	35
	TN	0.230	5.9	214	118
Cu^{+} (77)	AN	0.20	4	199	40
		0.204	4	200	36
	PY	0.18	4	206	40
		0.202	4	205	36
	4MPY	0.191	3.9	205	36
	2MPY	0.191	3.1	201	36
	26DMPY	0.195	3.0	201	36
Cu^{2+} (73)	AN	1.06×10^{-3}	4[d)]	199[d)]	127
			2[e)]	240[e)]	
		9.95×10^{-2}	4[d)]	200[d)]	127
			2[e)]	249[e)]	
		0.498	4[d)]	199[d)]	128
			2[e)]	218[e)]	
		1.00	4[d)]	199[d)]	40
	PY	0.498	4[e)]	204[e)]	128
	NH_3	0.4	4[d)]	200[d)]	129
			1[e)]	196[e)]	
	PA	0.350	4[d)]	204[d)]	18
			2[e)]	238[e)]	
	EN	0.500	4[d)]	204[d)]	116
			2[e)]	239[e)]	
	TN	0.229	4[d)]	204[d)]	18
			2[d)]	251[e)]	
Zn^{2+} (74.0)	AN	0.198	6	213	18
	4MPY	0.1	3.7	203	38
Pd^{2+} (86)	AN	0.447	4.0	200	18
Ag^{+} (115)	AN	0.2	3.7	224	41
		0.399	3.7	229	16
	PY	0.2	3.9	229	41
	2MPY	0.517	3.9	230	16
	NH_3	0.2	3.7	231	41
	PA	0.367	3.8	229	16
	EN	0.364	4.1	231	16
Cd^{2+} (95)	AN	0.3	6.3	235	18
Pt^{2+} (80)	AN	0.47	4.0	200	20
Au^{+} (137)	AN	0.060	4	219	42
	PY	0.040	4	216	42

a) Each figure in parenthesis is the effective ionic radius in pm. Ref. 25. b) The integer number means that the solvation number is fixed. c) 6- and 4-coordinate structures are mixed. d) Equatorial site. e) Axial site.

because the σ-donation of solvent molecules partly neutralizes the positive charge on the Co^{2+} ion, leading to an increase in the electronic repulsion on the Co^{2+} ion and a decrease in the attractive interaction between Co^{2+} and solvent molecules.

(2) Effect of the Kind of Donating Nitrogen Atoms. In marked contrast to the oxygen-donating solvents, there is a large variation in the M–N bond lengths even if the solvation numbers are the same. The nitrogen-donating solvents are classified into three categories on the basis of the kind of donating nitrogen atoms: i.e., (i) aliphatic amines with the sp^3-hybridizing nitrogen, such as NH_3, EN, TN, and PA; (ii) pyridine derivatives with the sp^2-hybridizing nitrogen, such as PY, 4MPY, 3MPY, 2MPY, and 26DMPY; and (iii) nitriles with the sp-hybridizing nitrogen, such as AN, PN, BuN, *i*BuN, BzN, and VN. The average M–N bond lengths for each group of solvents are summarized in Table 4. According to the *r* values in Table 4, the M–N bond lengths tend to decrease with the increasing p character for the σ-donating orbital on the nitrogen atom, i.e., the *r* values are in the order of M–N(sp^3) > M–N(sp^2) > M–N(sp). This order corresponds to the expanding extent of the lone pair orbital, which is the largest for N(sp^3) and gradually decreases to N(sp) with the decreasing p character.

(3) Solvation of Monovalent Metal Ions. The 4-coordinate tetrahedral solvation structure is ovserved for the monovalent metal ions, such as Cu^+,[36,40] Ag^+,[16,41] and Au^+,[42] regardless of the large ionic radius, not only in the nitrogen-donating solvents but also in the oxygen-donating solvents. The selection of the solvation number of 4 is quantitatively confirmed by the ab initio molecular orbital calculations about the solvation reactions (Eq. 8), in which the formation of a solvated metal ion ($[MS_n]^+$; M = Cu and Ag) in solvent S is decomposed into virtual stepwise solvation steps.

$$M^+ + nS \rightarrow [MS_n]^+ \quad (8)$$

The electronic stabilization energy (ΔE_{solv}) for Eq. 8 is given by Eq. 9,

$$\Delta E_{solv} = E_{MS_n} - (E_M + nE_S) + \Delta E_{BSSE} \quad (9)$$

where E_{MSn}, E_M, and E_S are the electronic energies, calculated using the Gaussian programs,[43,44] of the solvated metal ion, the free metal ion, and the free solvent, respectively. ΔE_{BSSE} denotes the basis set superposition error, which is estimated by the Boys–Bernardi counterpoise method,[45] between the metal ion and solvent molecules in $[MS_n]^+$. All bond lengths and angles were optimized in order to obtain the most stable structure during the quantum mechanical calculations, and the frequency analysis was carried out to confirm that the obtained structure is located at the local minimum on the potential energy surface and to obtain the values of the internal energy change (ΔU_{solv}) and the entropy change (ΔS_{solv}). The enthalpy change (ΔH_{solv}) was then calculated using the ΔE_{solv} and ΔU_{solv} values, and the value of the Gibbs free energy change (ΔG_{solv}) was obtainable using the ΔH_{solv} and ΔS_{solv} values.

Table 4. M–N Bond Lengths for Solvated Metal Ions in Nitrogen Donating Solvents

Metal	r[a)]/pm		
	N(sp^3)	N(sp^2)	N(sp)
Mn^{2+}	228 (7)	225 (4)	221
Fe^{2+}	222 (8)		214
Co^{2+}	217 (6)	215 (4)	211
Ni^{2+}	213 (6)	211 (4)	207
Cu^+		205 (5)	200
Cu^{2+} [b)]	204 (5)	224 (5)	199
Ag^+	231 (7)	230 (6)	224

a) Each figure in the parenthesis denotes the difference in *r* relative to *r* in the solvents with the sp-type donating nitrogen. b) At the equatorial site.

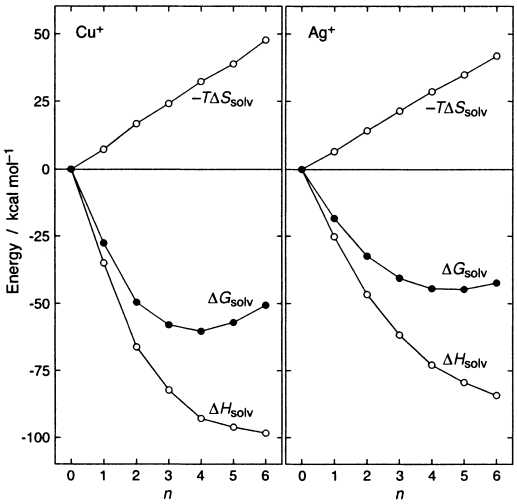

Fig. 6. Variations in ΔG_{solv}, ΔH_{solv}, and $-T\Delta S_{solv}$ at 298 K and 1 atm as a function of solvation number *n* for $[Cu(NCH)_n]^+$ and $[Ag(NCH)_n]^+$.

As pointed out above, the strong σ-donating ability of the solvent molecule tends to reduce the solvation number. However, the 4-coordinate solvation structure for monovalent metal ions is observed in all solvents, including AN with a weak σ-donating ability. This characteristic was clearly proved by a series of ab initio molecular orbital calculation of $[Cu(NCH)_n]^+$ and $[Ag(NCH)_n]^+$ (n = 0–6), where HCN is regarded as a model of AN with the weakest σ-donating property.[16,36] The calculated values of ΔG_{solv}, ΔH_{solv}, and $-T\Delta S_{solv}$ at 298 K and 1 atm are depicted in Fig. 6 as a function of *n*. The $-T\Delta S_{solv}$ value simply increases with increasing *n*. On the other hand, although the enthalpy term monotonically stabilizes the product side of Eq. 8 together with increasing *n*, the difference in ΔH_{solv} between $[M(NCH)_{n-1}]^+$ and $[M(NCH)_n]^+$ becomes gradually smaller. This is interpreted in terms of the many-body effect due to the partial neutralization of the positive charge on M^+ and the increase in the electrostatic repulsions between the negative charges on the coordinating nitrogen atoms. The ΔG_{solv} values then show a minimum at n = 4 as a consequence of the compensation of ΔH_{solv} by the entropy term for both metal ions. The curvature of ΔG_{solv} around the minimum value is greater for Cu^+ than Ag^+, reflecting the shorter Cu–N bond length and thus the larger many-body effect in the case of Cu^+.

3. Solvent Exchange Reactions of Metal Ions

The solvent exchange is the most fundamental chemical reaction that occurs around the metal ions in solution. Here, some characteristics observed in the solvent exchange rates are presented and their mechanistic aspects are discussed, referring to the results of the solvation structures described above.

3.1. Determination of Rate Constants and Activation Parameters for Solvent Exchange Reaction by NMR Technique. The nuclear magnetic resonance (NMR) technique is the most powerful tool to determine the rate constants of the solvent exchange reactions without a free energy change. The slow exchange reactions ($\tau_{1/2} \geq 1$ h) can be followed using the isotope dilution technique in the same sense as usual spectrophotometric methods, e.g., after $[M(D_2O)_n]^{m+}$ is dissolved in H_2O, an increase in the ^1H NMR peak intensity of the bound H_2O molecules as a function of time is analyzed using the McKay equation[46] to determine the water exchange rate constant. In the case of fast exchange reactions, there are two adoptable techniques, according to the magnetic property of the metal ion. For the diamagnetic metal ions, the line shape of the NMR spectrum for the solution containing the metal ion, in which two kinds of NMR lines corresponding to the solution containing the metal ion, in which two kinds of NMR lines corresponding to the bound and bulk solvent molecules appear, is analyzed by the two-site exchange model.[47–49] In this case, it is necessary to dilute the solvent concentration using an inert medium; otherwise the NMR peak of the bound solvent molecules may be hidden in the corresponding intense peak of the bulk solvent.

The solvent exchange rate constant of the paramagnetic metal ions can be determined by measuring the enhanced transverse relaxation rate (T_{2P}^{-1}) and the frequency shift ($\Delta\omega_P$) caused by the paramagnetic metal ion for the NMR signal of the bulk solvent. These quantities are determined as the difference between the corresponding values in the presence and absence of the metal ion, as expressed by Eqs. 10 and 11.

$$T_{2P}^{-1} = \pi(\Delta\nu_s - \Delta\nu_r) \tag{10}$$

$$\Delta\omega_P = 2\pi(\omega_s - \omega_r) \tag{11}$$

where $\Delta\nu$ and ω are the half-height width and the peak frequency of the bulk solvent, respectively; the subscripts "s" and "r" represent the sample in the presence and absence of the paramagnetic nuclei, respectively. Since the T_{2P}^{-1} and $\Delta\omega_P$ values are proportional to the mole ratio (P_M) of the bound solvent molecules relative to the solvent molecules in the bulk, they are divided by P_M defined as $n[M]/([S] - n[M])$, where n is the solvation number of the metal ion, [M] is the molality of the metal ion, and [S] is the molality of the solvent. Under only one requirement, $P_M \ll 1$, the values of $(T_{2P}P_M)^{-1}$ and $\Delta\omega_P P_M^{-1}$ are expressed by the so-called Swift–Connick equations (Eqs. 12 and 13),[47,50–52]

$$(T_{2P}P_M)^{-1} = \tau_M^{-1}\frac{T_{2M}^{-1}(T_{2M}^{-1} + \tau_M^{-1}) + \Delta\omega_M^2}{(T_{2M}^{-1} + \tau_M^{-1})^2 + \Delta\omega_M^2} + T_{2O}^{-1} \tag{12}$$

$$\Delta\omega_P P_M^{-1} = \frac{\Delta\omega_M}{(1 + T_{2M}^{-1}\tau_M)^2 + (\tau_M\Delta\omega_M)^2} \tag{13}$$

where τ_M is the mean residence time of the bound solvent molecule, T_{2M}^{-1} is the transverse relaxation rate of the bound solvent molecules, $\Delta\omega_M$ is the difference in the frequency between the bound and bulk solvents, and T_{2O}^{-1} is the transverse relaxation rate of the bulk solvent. These values are measured as a function of temperature and pressure, and the activation enthalpy ($\Delta^{\ddagger}H^{\circ}$), the activation entropy ($\Delta^{\ddagger}S^{\circ}$), and the activation volume ($\Delta^{\ddagger}V^{\circ}$) of the solvent exchange reaction are determined using the temperature and pressure dependences of τ_M^{-1} ($= k_{ex}$: solvent exchange rate constant) expressed by Eqs. 14 and 15.

$$k_{ex} = \tau_M^{-1} = \frac{k_B T}{h}\exp\left(-\frac{\Delta^{\ddagger}H^{\circ}}{RT} + \frac{\Delta^{\ddagger}S^{\circ}}{R}\right) \tag{14}$$

$$k_{ex} = \tau_M^{-1} = k_{ex}^{0}\exp\left(-\frac{\Delta^{\ddagger}V^{\circ}}{RT}P + \frac{\Delta^{\ddagger}\beta}{2RT}P^2\right) \tag{15}$$

where k_B is the Boltzman constant, R is the gas constant, k_{ex}^{0} is the solvent exchange rate constant at $P = 0$, and $\Delta^{\ddagger}\beta$ is the isothermal compressibility coefficient of activation. According to Eq. 12, the measured $(T_{2P}P_M)^{-1}$ values correspond to τ_M^{-1} under the conditions of $T_{2M}^{-1} \gg \tau_M^{-1} \gg T_{2O}^{-1}$, and the $\Delta^{\ddagger}H^{\circ}$ and $\Delta^{\ddagger}S^{\circ}$ values are thus directly determined by the temperature dependence of $(T_{2P}P_M)^{-1}$. By the variable-pressure measurements at such temperatures using the high-pressure NMR instrument,[53,54] the $\Delta^{\ddagger}V^{\circ}$ and $\Delta^{\ddagger}\beta$ values can be determined. However, if such conditions ($(T_{2P}P_M)^{-1} \sim \tau_M^{-1}$) are not established, the expressions of the temperature and pressure dependence for the T_{2M}^{-1},[48,49,55–58] $\Delta\omega$M,[59–62] and T_{2O}^{-1} terms[63,64] contained in Eqs. 12 and 13 are necessary in order to determine the activation parameters of the solvent exchange reaction.

3.2. Water Exchange Reactions. The water exchange on metal ions is the most basic ligand substitution reaction of the metal ions in water. Here, the mechanisms for the exchange reaction are discussed from the experimental and theoretical points of view.

(1) Experimental Investigations. The rate constants and the activation parameters for the water exchange on many metal ions are determined using the NMR technique.[65] Especially, the $\Delta^{\ddagger}V^{\circ}$ values have been mainly measured by Merbach et al., who proposed the mechanisms on the basis of the $\Delta^{\ddagger}V^{\circ}$ values. The Langford–Gray classification of the reaction mechanisms is originally applied to a series of ligand substitution rates of a certain metal ion. If the reaction rates are independent of the nature of the entering ligands, as in the case of Ni^{2+} and Co^{2+},[65] the reaction mechanism is concluded to be dissociative. Contrary, if the rates are dependent on the kinds of entering ligands, as in the case of Pd^{2+} and Be^{2+},[65] the associative mode of activation is assigned. The early works by Merbach et al. to determine the $\Delta^{\ddagger}V^{\circ}$ values for these metal ions, of which the mechanisms have well been characterized, strongly indicate that the activation volume becomes a good measure for the reaction mechanism. The $\Delta^{\ddagger}V^{\circ}$ term is represented as $\Delta^{\ddagger}V_{int}^{\circ} + \Delta^{\ddagger}V_{el}^{\circ}$, where $\Delta^{\ddagger}V_{int}^{\circ}$ is the intrinsic volume difference between the transition and ground states and $\Delta^{\ddagger}V_{el}^{\circ}$ is the contribution from the electrostriction of solvents caused by the change in charge distribution in the transition state. Since the contribution of $\Delta^{\ddagger}V_{el}^{\circ}$ is regarded as zero for the solvent ex-

change reactions without any formal charge difference between the reactants and the products, the observed $\Delta^{\ddagger}V^{\circ}$ value becomes identical to $\Delta^{\ddagger}V^{\circ}_{int}$, which includes the volume change caused by bond-making with the entering solvent molecule and by bond-breaking with the leaving solvent molecule. Therefore, the sign and the magnitude of $\Delta^{\ddagger}V^{\circ}$ are connected to the mechanistic behaviors. A positive $\Delta^{\ddagger}V^{\circ}$ value means the dissociation of a water molecule from the first hydration sphere by the dissociative mode of activation, while the associative mechanism with the interpenetration of an entering water molecule into the first hydration sphere is supported by a negative $\Delta^{\ddagger}V^{\circ}$ value. The $\Delta^{\ddagger}V^{\circ}$ value of zero implies the compensation of volume expansion due to the leaving water molecule by volume contraction due to the entering water molecule, thus showing the interchange mechanism. Recently, it has been theoretically confirmed that such criteria based on the activation volumes are acceptable for the water exchange reactions (see succeeding theoretical part). The water exchange rate constants (k_{ex}) and the activation parameters are summarized in Table 5.

The water exchange of the octahedrally hydrated main group metal ions, such as Mg^{2+}, Al^{3+}, and Ga^{3+}, are assigned to proceed via the dissociative interchange mechanism, since their $\Delta^{\ddagger}V^{\circ}$ values are positive.[65–67] The mechanism of the smallest and tetrahedrally hydrated Be^{2+} ion is associative based on the $\Delta^{\ddagger}V^{\circ}$ value of -13.6 cm^3 mol^{-1}.[68] In the case of Pd^{2+} and Pt^{2+} with the 4-coordinate square-planar hydration structure, the water exchange reaction is considered to proceed via the 5-coordinate trigonal bipyramidal intermediate by the associative mode of activation, as supported by their negative $\Delta^{\ddagger}V^{\circ}$ values.[69,70] The negative $\Delta^{\ddagger}V^{\circ}$ values of all trivalent transition metal ions including the lanthanide(III) ions listed in Table 5 support the associative or associative interchange mechanisms.[71–78]

For a series of divalent first-row transition metal ions (V^{2+}, Mn^{2+}, Fe^{2+}, Co^{2+}, Ni^{2+}, and Cu^{2+}), Merbach et al. have pointed out that the $\Delta^{\ddagger}V^{\circ}$ values of their water exchange reactions change from negative to positive with the increasing atomic number along this series,[79–82] i.e., the mechanistic changeover from associative interchange to dissociative interchange. This changeover is explained by the decrease in the ionic radius and the increase in the number of 3d electrons, i.e., the associative approach of an entering water molecule is unfavorable for smaller metal ions due to the steric crowdedness, and the dissociative activation becomes favorable for later members with more 3d electrons due to the electrostatic repulsion between

Table 5. Rate Constants and Activation Parameters of Water Exchange Reactions Determined by NMR Technique

Metal	k_{ex} [a] / s^{-1}	$\Delta^{\ddagger}H^{\circ}$ / kJ mol^{-1}	$\Delta^{\ddagger}S^{\circ}$ / J mol^{-1} K^{-1}	$\Delta^{\ddagger}V^{\circ}$ / cm^3 mol^{-1}	Reference
Divalent metal ions					
Be^{2+}	7.3×10^2	59.2	8.4	−13.6	68
Mg^{2+}	6.6×10^5	49.4	32.3	+6.0	65
V^{2+}	87	61.8	−0.4	−4.1	79
Mn^{2+}	2.1×10^7	32.9	5.7	−5.4	80
Fe^{2+}	4.4×10^6	41.4	21.2	+3.8	80
Co^{2+}	3.2×10^6	46.9	37.2	+6.1	80
Ni^{2+}	3.2×10^4	56.9	32.0	+7.2	53,80
Cu^{2+}	4.4×10^9	11.5	−21.8	+2.0	81,82
Ru^{2+}	1.8×10^{-2}	87.8	16.1	−0.4	75
Pd^{2+}	5.6×10^2	49.5	−26	−2.2	69
Pt^{2+}	3.9×10^{-4}	89.7	−9	−4.6	70
Trivalent metal ions					
Al^{3+}	1.29	84.7	41.6	+5.7	66
Ti^{3+}	1.8×10^5	43.4	1.2	−12.1	71
V^{3+}	5.0×10^2	49.4	−27.8	−8.9	72
Cr^{3+}	2.4×10^{-6}	108.6	11.6	−9.6	130
Fe^{3+}	1.6×10^2	64.0	12.1	−5.4	73,74
Ga^{3+}	4.0×10^2	67.1	30.1	+5.0	67
Ru^{3+}	3.5×10^{-6}	89.8	−48.3	−8.3	75
Rh^{3+}	2.2×10^{-9}	131	29	−4.2	76
In^{3+}	4.0×10^4	19.2	−96		131
Gd^{3+}	8.3×10^8	14.9	−24.1	−3.3	113
Tb^{3+}	5.6×10^8	12.1	−36.9	−5.7	77
Dy^{3+}	4.3×10^8	16.6	−24.0	−6.0	77
Ho^{3+}	2.1×10^8	16.4	−30.5	−6.6	77
Er^{3+}	1.3×10^8	18.4	−27.8	−6.9	77
Tm^{3+}	9.1×10^7	22.7	−16.4	−6.0	77
Yb^{3+}	4.7×10^7	23.3	−21.0		77
Ir^{3+}	1.1×10^{-10}	130.5	2.1	−5.7	78

a) Water exchange rate constant at 298 K.

the d electrons of the metal ion and the lone pair electrons of the entering and leaving water molecules.[65,80] Similarly, the water exchange on the trivalent metal ions (Ti^{3+}, V^{3+}, Cr^{3+}, Fe^{3+}, and Ga^{3+}) becomes less associative from Ti^{3+} ($\Delta^{\ddagger}V^{\circ} = -12.1$ cm^3 mol^{-1}) to Fe^{3+} (-5.4 cm^3 mol^{-1}) and becomes a dissociative interchange for Ga^{3+} ($+5.0$ cm^3 mol^{-1}) with the smallest ionic radius and the most 3d electrons.

(2) Theoretical Investigations. The water exchange mechanisms of hydrated metal ions are investigated by the theoretical approach using ab initio molecular orbital calculations.[83–93] For the water exchange reaction of the hexaaqua metal ions ($[M(OH_2)_6]^{m+}$), the structural and electronic properties of the species with the reduced and expanded hydration number (pentaaqua $[M(OH_2)_5]^{m+}$ and heptaaqua $[M(OH_2)_7]^{m+}$) are calculated as the transition state or the intermediate. The vibrational properties of these species are crucial pieces of information to judge the reaction mechanism. If the species is located at the second- or higher-order saddle point on the potential energy surface, the reaction pathway through the species can be perfectly ruled out. Because the pentaaqua species are located at the local minimum for all 3d block metal ions,[84–88] the vibrational properties of a series of heptaaqua species are quite important for estimating the pathway of the water exchange reaction. The vibrational nature of the stationary point for the heptaaqua $[M(OH_2)_7]^{m+}$ ($m = 2$ and 3) species is summarized in Table 6.[90–93] The $[M(OH_2)_7]^{m+}$ species with the d^0, d^1, and d^2 electronic configurations are at the local minima, the d^3 and d^4 species are at the saddle points, the d^5 species is at the local minimum, the d^6 and d^7 species are at the saddle points, and the d^8, d^9, and d^{10} species are at the second-order saddle points. These findings clearly indicate that the structural stability of $[M(OH_2)_7]^{m+}$ depends on the number of d electrons and their configurations.

The molecular orbitals formed by the σ interaction between the d orbitals of the metal ion and the ligand group orbitals in $[M(OH_2)_7]^{m+}$ are schematically depicted in Fig. 7 together with their energy levels. Since the optimized structure of $[M(OH_2)_7]^{m+}$ is not a regular pentagonal bipyramidal (in D_{5h} symmetry) but in C_2 symmetry, there is no degeneracy between these molecular orbitals. The vibrational nature of $[M(OH_2)_7]^{m+}$ is then decided by the occupation of the $b^{(2)}$, $a^{(2)}$, and $a^{(3)}$ orbitals with the antibonding characteristics for the σ

Table 6. Vibrational Nature of Stationary Point for Heptaaqua $[M(OH_2)_7]^{m+}$ ($m = 2$ and 3) Obtained by Ab Initio Molecular Orbital Calculation

	$[M(OH_2)_7]^{2+}$		$[M(OH_2)_7]^{3+}$	
d^0	Ca^{2+}	local minimum	Sc^{3+}	local minimum
d^1	Sc^{2+}	local minimum	Ti^{3+}	local minimum
d^2	Ti^{2+}	local minimum	V^{3+}	local minimum
d^3	V^{2+}	saddle point	Cr^{3+}	saddle point
d^4	Cr^{2+}	saddle point	Mn^{3+}	saddle point
d^5	Mn^{2+}	local minimum	Fe^{3+}	local minimum
d^6	Fe^{2+}	saddle point	Co^{3+}	saddle point
d^7	Co^{2+}	saddle point		
d^8	Ni^{2+}	2nd-order saddle point		
d^9	Cu^{2+}	2nd-order saddle point		
d^{10}	Zn^{2+}	2nd-order saddle point		

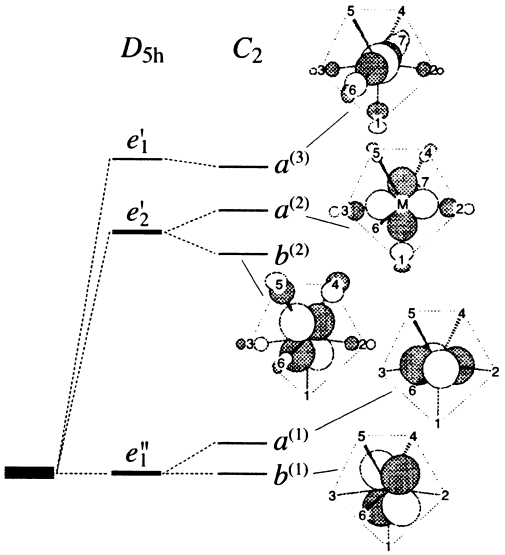

Fig. 7. Schematic diagram of the energy levels and molecular orbitals formed by the interaction between the σ orbitals of the water molecules and the d orbitals of the metal ion in $[M(OH_2)_7]^{m+}$ ($m = 2$ and 3).

interaction.[92,93] The Ca^{2+}, Sc^{2+}, Ti^{2+}, Sc^{3+}, Ti^{3+}, and V^{3+} ions with the vacant antibonding orbitals can be at the local minima on the potential energy surface. The single occupation of the $b^{(2)}$ orbital (V^{2+} and Cr^{3+}) generates a transition probability for the asymmetric distortion to make one water molecule closer to and the other more distant from the metal ion. This transition probability is caused by the interaction between the $b^{(2)}$ orbital and the lowest unoccupied 4s orbital of the metal ion. Similarly, the further occupation of the $a^{(2)}$ orbital (Cr^{2+} and Mn^{3+}) produces a transition probability to make one water molecule closer to and two water molecules more distant from the metal ion due to the interaction with the 4s orbital. Thus, the heptaaqua $[M(OH_2)_7]^{m+}$ species of these metal ions are at the saddle point on the potential energy surface, and this is the case for the Fe^{2+}, Co^{2+}, and Co^{3+} ions. Two kinds of transition probabilities occur by the double occupation of the antibonding orbitals (Ni^{2+}, Cu^{2+}, and Zn^{2+}), and their $[M(OH_2)_7]^{m+}$ species standing at the second-order saddle point. An exception is seen in the case of the d^5 metal ions (Mn^{2+} and Fe^{3+}), for which the$[M(OH_2)_7]^{m+}$ species are at the local minimum. In these cases, the efficient mixing of the orbitals and the largest Coulombic interactions between the metal ion and the water molecules among the series make the structure distortion quite unfavorable.[92]

According to the structural stability of the heptaaqua $[M(OH_2)_7]^{m+}$ species discussed above, the A, I_a, I, and I_d pathways for the Ni^{2+}, Cu^{2+}, and Zn^{2+} ions are completely ruled out, because their $[M(OH_2)_7]^{m+}$ species are at the second-order saddle points, which are not chemically relevant stationary points, and thus their water exchange reactions should proceed via the D mechanism. On the other hand, the A and/or I_a mechanisms are acceptable for the early members of the 3d-block metal ions, such as Sc^{2+}, Ti^{2+}, Ti^{3+}, and V^{3+}, with the vacant antibonding *a* and *b* orbitals and also for the Mn^{2+} and Fe^{3+} ions with the d^5 electronic configuration.

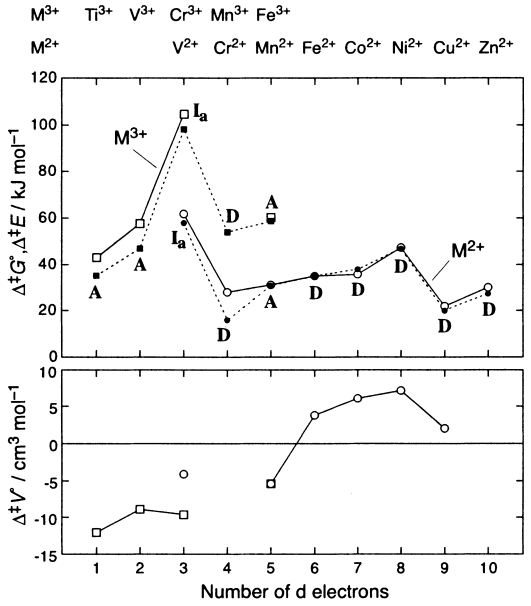

Fig. 8. The values of $\Delta^{\ddagger}E$ (filled markers) computed by the molecular orbital calculations and $\Delta^{\ddagger}G°$ at 298 K (open markers) determined by the NMR technique for the 3d-block divalent (circles) and trivalent (squares) metal ions. The mechanistic characterizations (A, I_a, and D) on the basis of the theoretical calculations are given in the upper panel. In the lower panel, the $\Delta^{\ddagger}V°$ values determined by the high-pressure NMR technique are plotted.

Furthermore, the reaction mechanisms can be estimated on the basis of the calculated energy difference ($\Delta^{\ddagger}E$) between the ground state $[M(OH_2)_6]^{m+}$ and the possible transition state, i.e., a pathway having the smallest $\Delta^{\ddagger}E$ value should be selected for the activation. The smallest $\Delta^{\ddagger}E$ values calculated by Rotzinger and the $\Delta^{\ddagger}G°$ values determined experimentally at 298 K are plotted for the 3d-block divalent and trivalent metal ions in Fig. 8,[86,87] in which the estimated $\Delta^{\ddagger}G°$ values for the complexation rates of Cr^{2+} [94] and Zn^{2+} [95] are included. The $\Delta^{\ddagger}E$ values reproduce well the $\Delta^{\ddagger}G°$ values determined by the NMR technique for all metal ions given in Fig. 8. Impressively, the sign of the $\Delta^{\ddagger}V°$ values determined by the high-pressure NMR technique is perfectly in accordance with the mechanistic conclusions of the quantum mechanical calculations, i.e., the $\Delta^{\ddagger}V°$ values for the metal ions (Fe^{2+}, Co^{2+}, Ni^{2+}, and Cu^{2+}) taking the D mechanism are positive and those for the metal ions (V^{2+}, Mn^{2+}, Ti^{3+}, V^{3+}, Cr^{3+}, and Fe^{3+}) taking the A or I_a mechanisms are certainly negative.

On the other hand, a variable pressure study of the water exchange on Ru^{2+} gave an activation volume close to zero (-0.4 cm^3 mol^{-1}) and this was interpreted as the I mechanism.[75] However, quantum mechanical calculations recently showed that the water exchange of Ru^{2+} follows the D mechanism.[96] In the case of the second-row transition metal(II) ion, Ru^{2+}, the volume contraction for forming the pentaaqua transition state is explained to be large enough to offset the increase in volume brought about by the dissociation. However, such phenomenon is not reported for the first-row transition metal ions.[86,87]

The transition states for the water exchange reaction via the I_a, I, or I_d mechanism have the entering and leaving water molecules in the *cis* or *trans* position to each other, i.e., a *cis* elimination or a *trans* elimination. The transition probability at the heptaaqua $[M(OH_2)_7]^{m+}$ (m = 2 and 3) species decides where the actual displacement occurs.[92,93] It has been first demonstrated that the V^{2+} and Cr^{3+} ions with d^3 configuration, of which the water exchange is activated by the I_a mechanism,[86,87] prefer the *cis* elimination to the *trans* during the associative process.[92,93]

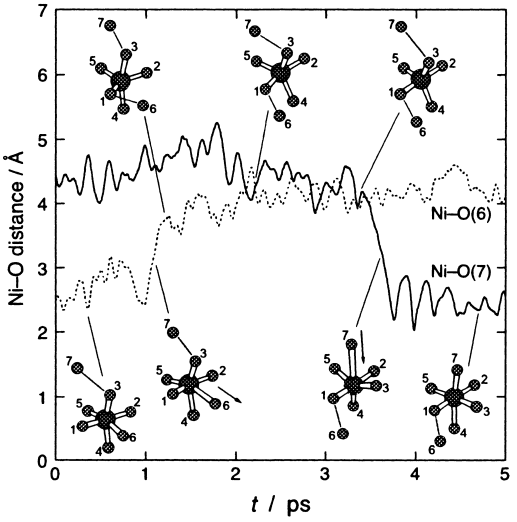

Fig. 9. Ni–O bond length trajectory for Ni–O pairs participating in the water exchange reaction calculated by MD simulation. Some instantaneous configurations of the NiO_7 fragment are included.

The other theoretical approach used to investigate the water exchange mechanism is the adoption of the molecular dynamics (MD) simulation. Recently, the MD simulation of the aqueous Ni^{2+} solution was carried out for a system composed of one Ni^{2+} ion and 499 water molecules at 298 K using the newly constructed ab initio two-body potential between Ni^{2+} and H_2O with the three-body corrections.[97] One water exchange reaction was observed during the MD simulation for a total of 6.0 ns, and the Ni–O bond length trajectory of two exchanging water molecules is shown in Fig. 9 together with some instantaneous configurations of the NiO_7 fragment. The water exchange reaction is initiated by structural distortion due to the repulsive interaction between one of the coordinating water molecules (labeled as 3 in Fig. 9) and an entering water molecule (7 in Fig. 9). The leaving water molecule (6 in Fig. 9) then dissociates from the Ni(II) ion to form the 5-coordinate intermediate. After the internal rearrangement of five water molecules (1–5 in Fig. 9) in the intermediate during its lifetime of ca. 2.5 ps, the entering water molecule (7 in Fig. 9) binds to the Ni(II) ion to form $Ni(OH_2)_6^{2+}$ again. This MD simulation clearly demonstrates that the water exchange reaction of Ni^{2+} is dissociative and that there is a distinct reaction intermediate with a reduced hydration number. However, it should be pointed out that the average interval time required for repeating such water exchange corresponds to the reciprocal of the water exchange rate constant; the rate constant is 3.2×10^4 s^{-1} (298 K) for water exchange of the Ni^{2+} ion.[53,80]

3.3. Bulkiness Effects of the Solvent Molecule on Solvent Exchange Mechanism. As in the case of the solvation struc-

ture, the structural bulkiness of the solvent molecule will influence the solvent exchange mechanism in two different ways. One effect is the steric crowdedness in the first solvation sphere due to the difference in bulkiness. This effect is important for the metal ion taking the associative mode of activation, since the steric crowdedness inhibits the entering of a solvent molecule. The other effect is due to the change in the solvation structure. As mentioned above, in a bulky solvent like TMU, the solvation number is changed in response to the ionic size, the ionic charge, and the d electron configuration of the metal ion. The change in the solvation number must have a significant influence upon the solvent exchange mechanism. Here, the former effect is first described on the basis of the systematic investigations of the solvent exchange kinetics of Ni^{2+} and Mn^{2+} in a series of nitriles (AN, PN, BuN, iBuN, BzN, and VN) and also on the basis of the activation parameters of Mn^{2+} in a variety of solvents, and then the latter is discussed according to the results of the TMU exchange reaction of Co^{2+}.

(1) Nitrile Exchange Reactions of Ni^{2+}. Since the metal hydrate and the water molecule are almost spherical, the $\Delta^{\ddagger}V^{\circ}$ value is determined by the balance between the positive and negative contributions due to the dissociation and association of the leaving and entering water molecules from and into the spherical first hydration sphere, respectively. Therefore, the value of $\Delta^{\ddagger}V^{\circ}$ is potentially a powerful measure to assign the mechanisms of the water exchange reactions (vide supra). However, since the substituent of the nitrile group has a complex structure, it is very important to define the "inner sphere" of the solvated metal ion in order to assess the magnitude of the $\Delta^{\ddagger}V^{\circ}$ values.[54] The inner sphere is defined as an effective sphere into which solvent molecules in the second solvation sphere cannot penetrate at the ground state, and it is definitely different from the first solvation sphere, in which all coordinating solvent molecules are included. The inner sphere of the hydrated metal ion is almost comparable to the first hydration sphere because of the small size and spherical shape of the water molecule, while most of the nitrile substituent overreaches the inner sphere of the hexasolvate in nitrile solvents. Such a redundant part is always on the outside of the inner sphere, and thus there is no contribution to the volume change by movement. The inner sphere and the $\Delta^{\ddagger}V^{\circ}$ value are illustrated for the general interchange mechanism in Fig. 10, in which only two exchanging solvent molecules are depicted for simplicity. During the activation process of the solvent exchange, one leaving solvent molecule dissociates from the metal ion to contribute to the positive volume as given by V_d, and the entering solvent molecule gets in the inner sphere to decrease the volume by V_a. In this transition state, the leaving and entering solvent molecules should become identical because of the microscopic reversibility. The value of $\Delta^{\ddagger}V^{\circ}$ is then represented as $V_d - V_a$, if there is no change in the size of the inner sphere during the activation.

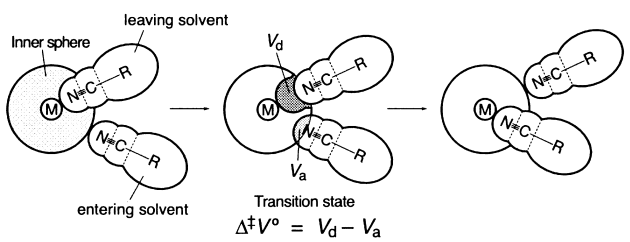

Fig. 10. Illustration for the inner sphere and the activation volume. The non-exchanging solvent molecules are omitted for simplicity. V_d and V_a denote the positive and negative contributions to the volume due to the leaving and entering solvent molecules, respectively.

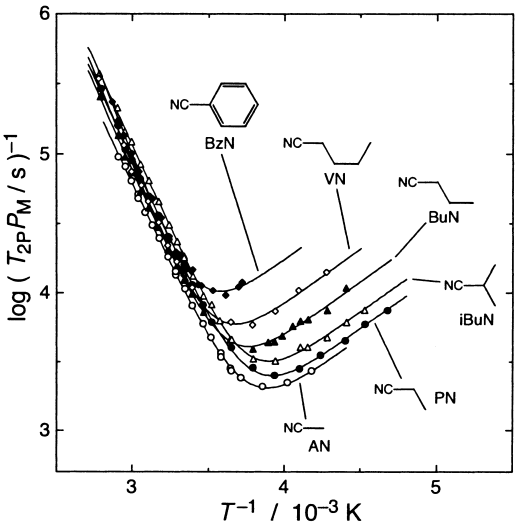

Fig. 11. Temperature dependence of $\log(T_{2P}P_M/s)^{-1}$ of the Ni^{2+} solutions in a series of nitriles.

The log $(T_{2P}P_M)^{-1}$ values determined by the ^{14}N NMR line broadening are shown in Fig. 11 for Ni^{2+} in a series of nitriles as a function of T^{-1}. In the temperature region where the log $(T_{2P}P_M)^{-1}$ values decrease with increasing T^{-1}, the observed transverse relaxation is governed by τ_M. The log $(T_{2P}P_M)^{-1}$ values begin to increase at much lower temperatures, indicating that the contribution of ${T_{2O}}^{-1}$ becomes predominant. The ${T_{2O}}^{-1}$ value at a certain temperature is then found to be in the order of AN $\leq$ PN $<$ *i*BuN $<$ BuN $<$ VN $<$ BzN, as seen from Fig. 11. It is well known that the ^{14}N NMR relaxation itself is governed by the electric quadrupolar interaction,[49] and the enhanced relaxation of the bulk nuclei due to the paramagnetic metal ion is also explained by the quadrupolar relaxation $({T_{2Q,O}}^{-1})$. The ${T_{2Q,O}}^{-1}$ value in the present system is expressed as Eqs. 16 and 17:[64]

$$ {T_{2Q,O}}^{-1} = F_Q\left(\frac{2r_M r_S}{r_2(r_M + r_S)} - \frac{r_A r_S}{r_3(r_A + r_S)}\right)\frac{\eta}{k_B T} \qquad (16) $$

$$ F_Q = \frac{192\pi^2\rho}{15}\left\{\frac{2\varepsilon + 3}{5\varepsilon}(1 - \varphi)\frac{e^2Q}{\hbar}\right\}^2 \frac{2I + 3}{I^2(2I - 1)} \qquad (17) $$

where r_M, r_A, and r_S denote the radius of the solvated metal ion, the counter ion, and the solvent, respectively, r_2 is the average distance of closest approach of the nucleus in the second solvation sphere of the metal ion, r_3 is the average distance of closest approach of the nucleus to the counter ion, η is the solvent viscosity, ρ is the solution density, ε is the dielectric constant of the solvent, φ is the Sternheimer antishielding factor representing the amplifying effect of inner electron motions on the applied electric field gradient, eQ is the nuclear electric quadrupole moment, e is the electron change, and I is the nu-

Table 7. Rate Constants at 298 K and Activation Parameters for Solvent Exchange Reactions of Ni^{2+} in a Series of Nitriles

Solvent	k_{ex}/s^{-1}	$\Delta^{\ddagger}H°$/kJ mol^{-1}	$\Delta^{\ddagger}S°$/J mol^{-1} K^{-1}	$\Delta^{\ddagger}V°$/cm^3 mol^{-1}
AN	6.2×10^3	41.4 ± 0.5	−30 ± 2	+12.4 ± 0.4
PN	1.3×10^4	42.0 ± 0.4	−25 ± 2	+13.7 ± 0.5
BuN	1.0×10^4	43.3 ± 0.7	−23 ± 2	+13.1 ± 0.5
iBuN	1.6×10^4	43.3 ± 0.5	−19 ± 2	+12.4 ± 0.6
VN	1.0×10^4	47.1 ± 1.2	−10 ± 4	+14.4 ± 0.4
BzN	9.4×10^3	51.6 ± 1.9	+4 ± 6	+13.1 ± 0.6

clear spin. According to Eqs. 16 and 17, if the values of r_2 and r_3 are available, the $T_{2Q,O}{}^{-1}$ value can be estimated using the standard geometry of the nitrile molecules. The used counter anion of the Ni^{2+} ion was $CF_3SO_3{}^-$, and the r_A value is estimated to be ca. 280 pm according to the van der Waals radii. The surface of $CF_3SO_3{}^-$ is composed of negatively charged atoms, and thus it is reasonable to assume that the nitrile molecules surround the anion with the antidipole alignment toward the anion center, leading to the r_3 value of $280 + 2r_S$, since the N atom is located at the negative end of the molecular dipole. If the inner sphere radius is then assumed to take the most reliable value of ca. 300 pm ($r_2 \sim 400$ pm) for all nitriles on the basis of the Ni–N bond length and the van der Waals radii, the ratio of the $T_{2Q,O}{}^{-1}$ values results in 1 (AN):1.5 (PN):2.3 (BuN):1.8 (iBuN):3.7 (VN):7.6 (BzN). This is in good agreement with the ratio of the observed $(T_{2P}P_M)^{-1}$ values of 1 (AN):1.2 (PN):2.6 (BuN):1.5 (iBuN):4.4 (VN):9.3 (BzN). Although the adoption of Eqs. 16 and 17 leads to a slight underestimation for BzN, in which an additional specific interaction between BzN and $CF_3SO_3{}^-$ is expected, not only the order but also the magnitude of the observed $(T_{2P}P_M)^{-1}$ values are well explained by the assumption of the same inner sphere radius for all nitrile solvates of Ni^{2+}. Since the bulkiness variation of a series of nitriles is due to the substituent group, which is far away from the metal center, the nitrile molecules in the second solvation sphere can penetrate into the gaps among the bound nitrile molecules without any steric influences. Under these conditions, the intrinsic volume change at the Ni^{2+} ion between the transition and ground states can be reflected in the $\Delta^{\ddagger}V°$ value.

In Table 7 are summarized the rate constants and activation parameters for the nitrile exchange reactions of Ni^{2+} determined by the ^{14}N NMR line-broadening technique.[54] The $\Delta^{\ddagger}V°$ values are largely positive and almost constant (ca. +13 cm^3 mol^{-1}) for a series of nitriles with a large variation in the substituent group. The inner sphere radius of 300 pm, which is supported by the observed $(T_{2P}P_M)^{-1}$ values in the $T_{2O}{}^{-1}$ -predominant region, means that the inner-sphere volume will be 68 cm^3 mol^{-1}, the observed $\Delta^{\ddagger}V°$ values almost correspond to the component of a single nitrile molecule (11 cm^3 mol^{-1}) in the inner sphere. This finding strongly indicates that the nitrile exchange reactions of Ni^{2+} proceed via the dissociative mechanism regardless of the difference in the substituent group. The leaving nitrile molecule is perfectly expelled from the inner sphere at the transition state, and the expected negative volume contribution by the entering nitrile molecule (V_a in Fig. 10) is negligible. In addition, the fact that the $\Delta^{\ddagger}V°$ values for a series of nitriles are almost the same suggests that any contributions to the volume in the second solvation sphere must be negligible.

On the other hand, the $\Delta^{\ddagger}H°$ values gradually increase in the order of AN < PN < BuN ~ iBuN < VN < BzN (see Table 7), while the $\Delta^{\ddagger}S°$ values become less negative in response to the increase in $\Delta^{\ddagger}H°$. Some physicochemical quantities reflecting the donating ability of the nitrile nitrogen, such as the Gutmann donor number[98] (14.1 (AN), 16.1 (PN), 16.6 (BuN), 15.4 (iBuN), and 11.9 (BzN)), the gas phase proton affinity[99] (188.4 kcal mol^{-1} (AN), 192.6 (PN), 193.7 (BuN), 194.3 (iBuN), 194.0 (VN), and 195.9 (BzN)), and the molecular dipole moment (3.53 D (AN), 3.50 (PN), 3.50 (BuN), 3.61 (iBuN), 3.57 (VN), and 4.01 (BzN)),[100] are almost comparable for a series of nitriles. Furthermore, the Ni–N bond lengths (207 pm) are constant for all nitriles (see Table 3). These comparable parameters mean that the strength of the Ni^{2+}–nitrile interaction is almost identical for all nitriles. Since the nitrile exchange is activated by the complete dissociation of a leaving nitrile molecule from the inner sphere, as described above, the change in $\Delta^{\ddagger}H°$ indicates the difference in the nature of solvent–solvent interactions in the second solvation sphere during the activation process. In the case of the smallest entry of AN, the solvent–solvent interaction is promoted by the interaction between molecular dipoles, which was confirmed by the X-ray diffraction study of pure AN.[101] This dipolar interaction may be largely affected by the structure and size of the substituent groups, and it is reasonably expected that the dipolar interaction between nitrile molecules becomes less feasible for the nitrile with a bulkier substituent. Thus, the smaller $\Delta^{\ddagger}H°$ value for the smaller nitrile reflects the more effective dipolar interaction between the leaving nitrile molecule and those in the second solvation sphere. Such dipolar interactions can lead to the more negative $\Delta^{\ddagger}S°$ value for the smaller nitrile (see Table 7).

(2) Solvent Exchange Reactions of Mn^{2+}. The water exchange reactoin of Mn^{2+} proceeds via the associative mode of activation and a negative $\Delta^{\ddagger}V°$ value (−5.4 cm^3 mol^{-1}) is reported.[80] The associative water exchange is also quantum-mechanically verified by the stable nature of the 7-coordinate species of Mn^{2+}.[87,92] Therefore, we can expect that the bulkiness of the solvent molecule will significantly affect the mechanisms of the solvent exchange on Mn^{2+} in comparison to Ni^{2+} with the dissociative mode of activation. The rate constants at 298 K and the activation parameters for the solvent exchange reactions of Mn^{2+} in a variety of solvents are summarized in Table 8.[34,53,80,102–107] As in the case of Ni^{2+}, the $\Delta^{\ddagger}V°$ values in a series of nitrile solvents with the different substituents are very useful to estimate the mechanistic difference that origi-

Table 8. Rate Constants at 298 K and Activation Parameters for Solvent Exchange Reactions of Mn^{2+} in Various Solvents

Solvent	k_{ex}/s^{-1}	$\Delta^{\ddagger}H°$/kJ mol^{-1}	$\Delta^{\ddagger}S°$/J mol^{-1} K^{-1}	$\Delta^{\ddagger}V°$/cm^3 mol^{-1}
AN[a)]	1.3×10^7	28.6	−13	−4.2[b)]
PN[a)]	1.3×10^7	29.6	−10	+0.7[b)]
BuN[a)]	9.9×10^6	31.3	−6	−0.6[b)]
iBuN[a)]	1.1×10^7	40.0	24	+2.5[b)]
VN[a)]	9.3×10^6	35.6	8	+1.8[b)]
BzN[a)]	1.2×10^7	36.9	14	
H_2O[c)]	2.1×10^7	32.9	5.7	−5.4
MeOH[d)]	3.7×10^5	25.9	−50.2	−5.0[e)]
DMSO[f)]	6.3×10^6	31	−10	
DMF[g)]	2.7×10^6	35.8	−2	+1.6
DMF[f)]	2.2×10^6	34.6	−7.4	+2.4[h)]
MBL[i)]	2.4×10^4	39	−25	
HOAc[j)]	1.6×10^7	29	−10	+0.4[k)]

a) Ref. 34. b) Values determined with the $\Delta^{\ddagger}\beta$ term in Eq. 15. c) Ref. 80. d) Ref. 132. e) Ref. 104. f) Ref. 105. g) Ref. 102. h) Ref. 106. i) *N*-methyl-γ-butyrolactam. Ref. 107. j) Ref. 103. k) Ref. 53.

nates from the solvent bulkiness.

In order to assess the $\Delta^{\ddagger}V°$ values, it is important to take into consideration the size of the inner sphere, as mentioned above. It is reasonable to assume that the size of the inner sphere around the Mn^{2+} ion is independent of the structure and size of the substituents of the cyano groups like the case of Ni^{2+}, because the Mn–N bond lengths are almost constant in all nitriles, which are longer by ca. 14 pm than the corresponding bond lengths for Ni^{2+} (see Table 3). The steric repulsion between the nitrile molecules in the first and second solvation spheres, expected when the nitrile molecules in the second solvation sphere penetrate into the gaps among the bound nitrile molecules in the ground state, is reduced by the more distant Mn–nitrile interaction in the first solvation sphere.

The $\Delta^{\ddagger}V°$ values for the solvent exchange of Mn^{2+} in a series of nitriles are significantly smaller than those of Ni^{2+}. Since the size of the inner sphere itself is not expected to be largely different between Mn^{2+} and Ni^{2+} according to the small difference between the M–N distances (ca. 14 pm), the smaller $\Delta^{\ddagger}V°$ values for Mn^{2+} indicate that there is an effective contribution of V_a due to the approach of an entering nitrile molecule in the transition state (see Fig. 10). The mechanism in the smallest AN is thus concluded to be I_a on the basis of the negative $\Delta^{\ddagger}V°$ value (-4.2 cm^3 mol^{-1}). The $\Delta^{\ddagger}V°$ values in other nitriles tend to increase with an increase in the bulkiness of the substituent. The mechanism becomes less associative due to the bulkiness of the substituent.

The $\Delta^{\ddagger}H°$ values of Mn^{2+} in a series of nitriles vary in response to the bulkiness of the solvent molecules. Since the mechanistic changeover from I_a to less associative is confirmed by the $\Delta^{\ddagger}V°$ values, the extent of bond making and bond breaking should appear in the $\Delta^{\ddagger}H°$ values. According to the hydration enthalpies (-1856 kJ mol^{-1} for Mn^{2+} and -2101 kJ mol^{-1} for Ni^{2+}),[108] the Mn–N bond enthalpy is roughly estimated to be ca. 90% of that for Ni^{2+}. By assuming that the contribution from the solvent–solvent interactions in the second solvation sphere is negligible in the case of bulky nitriles, such as VN and BzN, one can approximate the enthalpy loss for the Ni–N bond breaking as ca. 50 kJ mol^{-1} ($\Delta^{\ddagger}H°$ of Ni^{2+} in bulky nitriles, see Table 7), and one can estimate the corresponding value for Mn^{2+} to be ca. 45 kJ mol^{-1}. The $\Delta^{\ddagger}H°$ values of Mn^{2+} (ca. 36 kJ mol^{-1}, see Table 8) in such bulky solvents are significantly smaller than the estimated Mn–N bond breaking enthalpy, indicating the insufficient bond cleavage and the contribution of the bond making. Therefore, the smaller $\Delta^{\ddagger}H°$ value in less bulky nitriles corresponds to the more associative characteristic of the exchange mechanism.

The solvent exchange reactions of Mn^{2+} have been studied in other nonaqueous solvents as shown in Table 8.[53,103–107] The negative $\Delta^{\ddagger}V°$ values in small solvents, such as water,[80] AN,[34] and MeOH,[104] support the associative interchange mechanism. As clearly observed in a series of nitriles, the $\Delta^{\ddagger}V°$ value becomes more positive in bulky solvents, such as HOAc ($\Delta^{\ddagger}V° = +0.4$ cm^3 mol^{-1})[53] and DMF ($+1.6$ cm^3 mol^{-1}).[102] This suggests that the mechanism in HOAc and DMF is less associative than that in smaller solvents.

(3) Effects of Solvation Structure on Solvent Exchange Mechanism. If the solvation structure of the metal ion is changed due to the bulkiness of the solvent molecule, the solvent exchange reaction must be affected by the change. It is very important to clarify how the reaction mechanism varies when the solvation number is reduced in bulky solvents.

The rate constants at 298 K and the activation parameters for the solvent exchange reactions of Co^{2+} are summarized in Table 9.[32,52,80,103,109–111] The solvent exchange reaction in TMU is characterized by the smaller $\Delta^{\ddagger}H°$ and negative $\Delta^{\ddagger}S°$ values.[32] These parameters indicate the associative mode of activation for the 4-coordinate Co^{2+} ion in TMU. Since the Co–O bond length (200 pm) in TMU is shorter than those (208 pm) in the other solvents, in which the solvation structure is the 6-coordinate octahedral (see Table 1), much larger $\Delta^{\ddagger}H°$ values should be required, if the TMU exchange reaction is dissociative as in the other solvents. Furthermore, the d^7 electronic configuration of the high-spin Co^{2+} ion in the 4-coordinate solvate is favorable for the associative approach of the entering solvent molecule. In the case of the octahedral solvate, the

Table 9. Rate Constants at 298 K and Activation Parameters for Solvent Exchange Reactions of Co^{2+} in Various Solvents

Solvent	k_{ex}/s^{-1}	$\Delta^{\ddagger}H°$/kJ mol^{-1}	$\Delta^{\ddagger}S°$/J mol^{-1} K^{-1}	n[a)]
TMU[b)]	1.7×10^7	25.8	−20	4
H_2O[c)]	3.2×10^6	46.9	37.2	6
MeOH[d)]	1.8×10^4	57.7	30.1	6
AN[e)]	3.4×10^5	49.5	27.1	6
DMSO[f)]	4.5×10^5	49.0	28	6
DMF[g)]	3.9×10^5	56.9	52.7	6
HOAc[h)]	1.3×10^6	37	−6	

a) Solvation number. b) Ref. 32. c) Ref. 80. d) Ref. 52. e) Ref. 109. f) Ref. 110. g) Ref. 111. h) Ref. 103.

density distributions of the nonbonding t_{2g} orbitals spread toward the direction from which the entering solvent molecule accesses, and they are occupied by 5 electrons, while the number of electrons in the corresponding orbitals is reduced to 3 for the 4-coordinate Co^{2+} ion. This situation is much more favorable for the associative mode of activation. Consequently, the reduction in the solvation number caused by the bulkiness of the TMU molecule makes the solvent exchange mechanism more associative.

Similar behavior is also reported in the case of the 6-coordinate $[Al(OH_2)_6]^{3+}$, for which the dissociative interchange mechanism is proposed in water ($\Delta^{\ddagger}V° = +5.7$ cm^3 mol^{-1}),[66] while the HMPA exchange of the 4-coordinate $[Al(hmpa)_4]^{3+}$ is assigned to the associative mode of activation because of the linear dependence of rate constants on the HMPA concentration in a nitromethane diluent.[112]

The associative exchange is observed for the 4-coordinate Be^{2+} ion.[68] In water, the most negative $\Delta^{\ddagger}V°$ value (−13.6 cm^3 mol^{-1}) is almost in accordance with the difference (−12 cm^3 mol^{-1}) in the estimated partial molar volumes between $[Be(OH_2)_4]^{2+}$ and $[Be(OH_2)_5]^{2+}$, indicating the limiting associative mechanism. However, the $\Delta^{\ddagger}V°$ value becomes less negative in bulkier solvents: $\Delta^{\ddagger}V° = -2.5$ cm^3 mol^{-1} in DMSO, −3.1 in DMF, and −4.1 in TMP. These studies have been performed by the dilution of solvent, and the associative mechanism is confirmed by the linear dependence of the observed exchange rate constant on the solvent concentration. In much bulkier solvents, such as TMU and dimethylpropyleneurea, the observed rate constants are independent of the solvent concentration and the $\Delta^{\ddagger}V°$ value becomes large positive (+10.5 and +10.3 cm^3 mol^{-1}). These results clearly indicate the mechanistic changeover from associative to dissociative in response to the bulkiness of the solvent molecule for the 4-coordinate Be^{2+} ion. Judging from the results described above, one can conclude that the associative characteristic of the Co^{2+} ion in TMU indicates the deficient bulkiness of TMU for the 4-coordinate Co^{2+} solvate and reflects the unique solvation structure accompanying two strongly interacting TMU molecules in the second solvation sphere (vide supra).

The bulkiness of DMF and TMU affects the solvent exchange mechanisms of the lanthanide(Ⅲ) ions. The hydration structure of heavier members (Tb^{3+}–Lu^{3+}) is 8-coordinate square antiprismatic, and their water exchange reactions proceed by the associative mode of activation, judging from the small $\Delta^{\ddagger}H°$, negative $\Delta^{\ddagger}S°$, and negative $\Delta^{\ddagger}V°$ value (see Table 5).[77,113] In DMF, although the solvation numbers of Tb^{3+}–Yb^{3+} are the same as those in water, the $\Delta^{\ddagger}V°$ values become positive: +5.2 cm^3 mol^{-1} (Tb^{3+}), +6.1 (Dy^{3+}), +5.2 (Ho^{3+}), +5.4 (Er^{3+}), +7.4 (Tm^{3+}), and +11.8 (Yb^{3+}).[114] These positive $\Delta^{\ddagger}V°$ values are assigned to the dissociative mode of activation, and the more dissociative mechanism is pronounced for the heavier member with the smaller ionic radius. This mechanistic changeover is certainly due to the bulkiness of the DMF molecule. In a much bulkier solvent TMU, the 6-coordinate solvation structure is proposed for Tb^{3+}–Lu^{3+}, and the kinetic study of the TMU exchange reaction in the AN diluent revealed that the rate constant is independent of the concentration of TMU, i.e., the dissociative mechanism.[29] Although the solvation number of these lanthanide(Ⅲ) ions is reduced to 6 from the normal 8, the dissociative exchange seems to be forced by the steric hindrance in the first solvation sphere composed of six bulky TMU molecules.

3.4. Solvent Exchange Mechanism in Bidentate Solvents. In this section are described the kinetic investigations and the mechanistic interpretations for the solvent exchange reaction in bidentate solvents, such as EN and TN, which form the five- and six-membered chelate rings, respectively.[39,115–118]

One example of the temperature dependence of log $(T_{2P}P_M)^{-1}$ for Ni^{2+} in EN is shown in Fig. 12,[115] where the τ_M- and T_{2O}^{-1} -predominant regions are seen for ^1H (NH_2) (amine-proton), $^1H(CH_2)$ (methylene proton), ^{13}C, and ^{14}N. The fact that the $(T_{2P}P_M)^{-1}$ values in the τ_M-predominant region are independent of the observed nuclei means that the solvent exchange process of EN proceeds through the whole of a bidentate EN molecule. Because EN has two binding sites and the microscopic reversibility should be satisfied, the solvent ex-

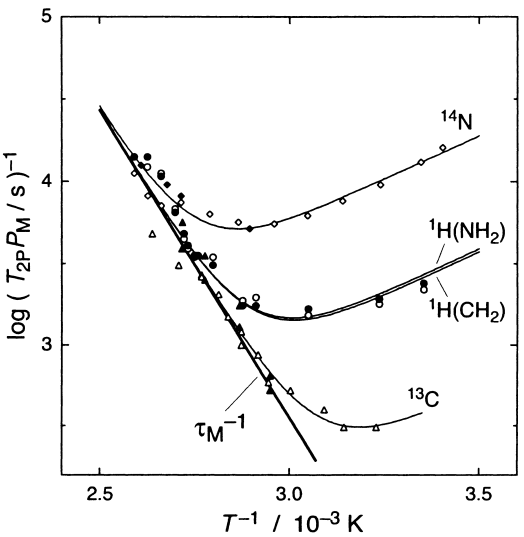

Fig. 12. Temperature dependence of $\log(T_{2P}P_M/s)^{-1}$ of methylene ^1H at 270 MHz (open circles), amine ^1H at 270 MHz (filled circles), ^{13}C at 67.89 MHz (open triangles), ^{14}N at 19.52 MHz (open diamonds), and ^{14}N at 7.20 MHz (filled diamonds) for Ni^{2+} in EN. The values of ^{13}C for 70.1% and 38.0% EN solution diluted by DMF are plotted by filled triangles. The solid line of τ_M^{-1} was calculated using the obtained values of $\Delta^{\ddagger}H°$ and $\Delta^{\ddagger}S°$.

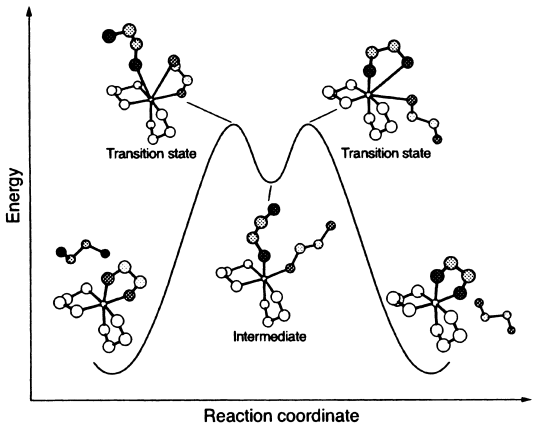

Fig. 13. Proposed mechanism for EN exchange reaction.

change reaction is considered to proceed via an intermediate, in which two EN molecules coordinate to the metal ion in the unidentate fashion, as shown in Fig. 13. The activation process corresponds to the replacement of one of two binding atoms of the leaving solvent by the first donating atom of the entering solvent. If the exchange reaction proceeds via the dissociative mechanism, there should be an additional intermediate with the reduced solvation number after the transition state.

The $(T_{2P}P_M)^{-1}$ value in the ${T_{2O}}^{-1}$ -predominant region is in the order of $^{14}N > {}^1H(NH_2) \sim {}^1H(CH_2) > {}^{13}C$ (see Fig. 12). In the case of the nuclei with $I = 1/2$ (^{1}H and ^{13}C), the ${T_{2O}}^{-1}$ term is governed by the dipolar relaxation (${T_{2D,O}}^{-1}$), expressed by Eqs. 18–20,[52,63]

$$ {T_{2D,O}}^{-1} = \frac{4\pi}{45}\frac{N_A[S]}{n}\frac{(\mu_B g_L \gamma_I)^2}{{r_2}^3}S(S+1)\left(7\tau_{d1,O} + \frac{13\tau_{d2,O}}{1+{\omega_S}^2{\tau_{d2,O}}^2}\right) \quad (18) $$

$$ {\tau_{d1,O}}^{-1} = {T_{1e}}^{-1} + {\tau_{D,MS}}^{-1} \quad (19) $$

$$ {\tau_{d2,O}}^{-1} = {T_{2e}}^{-1} + {\tau_{D,MS}}^{-1} \quad (20) $$

where N_A is the Avogadro constant, μ_B is the Bohr magneton, g_L is the Landé g factor of the solvated metal ion, γ_I is the magnetogyric ratio of the nucleus, S is the electron spin quantum number of the metal ion, ω_S is the Larmor angular frequency of electron, and T_{1e} and T_{2e} are the correlation times for the longitudinal and transverse electron relaxations of the metal ion, respectively. Thus, the observed $(T_{2P}P_M)^{-1}$ value at a certain temperature is proportional to $\gamma_I^2/{r_2}^3$, since all correlation times are the same for all the ^{1}H and ^{13}C nuclei. Almost consistent $(T_{2P}P_M)^{-1}$ values for $^1H(NH_2)$ and $^1H(CH_2)$ (see Fig. 12) mean similar r_2 values for these nuclei, and this implies the hydrogen bonding alignment of one amine nitrogen of the EN molecule in the second solvation sphere toward the amine proton of the coordinating EN molecule. Assuming such a configuration for the EN molecule in the second solvation sphere, one can reproduce the difference in the $(T_{2P}P_M)^{-1}$ values between ^{1}H and ^{13}C satisfactorily by taking the difference in γ_I into consideration. The adoption of a similar concept to the much larger $(T_{2P}P_M)^{-1}$ value of the ^{14}N nucleus with a much smaller γ_I results in an unreasonably short r_2 value. This means that the dipolar relaxation is a minor contribution (ca. 1% at most) for the ^{14}N nucleus with the electric quadrupole moment and that the ${T_{2O}}^{-1}$ term for the ^{14}N nucleus is governed by the quadrupolar relaxation (${T_{2Q,O}}^{-1}$).

The rate constants at 298 K and the activation parameters of the solvent exchange reactions in EN, TN, and PA for M^{2+} (M = Mn, Fe, Co, and Ni) are summarized in Table 10.[39,115,117,118] The $\Delta^{\ddagger}V^{\circ}$ value of Ni^{2+} in EN and TN are quite positive, indicating the dissociative mechanism as in water. The gradually decreasing $\Delta^{\ddagger}V^{\circ}$ values from Ni^{2+} to Mn^{2+} in both EN and TN suggest that the reaction mechanism becomes less dissociative in that order. The reaction mechanisms for the EN and TN exchanges are thus considered to be identical for each M^{2+}. However, as demonstrated in Fig. 14, the difference in k_{ex} between the EN and TN exchanges gradually increases from

Table 10. Rate Constants at 298 K and Activation Parameters for Solvent Exchange Reactions of Mn^{2+}, Fe^{2+}, Co^{2+}, and Ni^{2+} in EN, TN, and PA

Solvent	k_{ex}/s^{-1}	$\Delta^{\ddagger}H^{\circ}$/kJ mol^{-1}	$\Delta^{\ddagger}S^{\circ}$/J mol^{-1} K^{-1}	$\Delta^{\ddagger}V^{\circ}$/cm^3 mol^{-1}
		Mn^{2+}		
EN[a)]	1.7×10^6	27.7	−43	−0.6
TN[b)]	2.5×10^6	21.9	−50	+0.1
PA[b)]	3.7×10^7	26.2	−13	
		Fe^{2+}		
EN[a)]	4.3×10^4	46.3	−1	−1.2
TN[b)]	3.9×10^5	47.9	23	+5.8
PA[b)]	6.9×10^7	32.4	14	
		Co^{2+}		
EN[a)]	5.4×10^3	56.5	16	+0.9
TN[c)]	2.9×10^5	49.3	25	+6.6
PA[c)]	2.0×10^8	36.2	35	
		Ni^{2+}		
EN[d)]	19.6	69	10	+11.4
TN[b)]	3.1×10^3	61.3	28	+7.2
PA[b)]	1.3×10^7	37.1	16	

a) Ref. 117. b) Ref. 118. c) Ref. 39. d) Ref. 115.

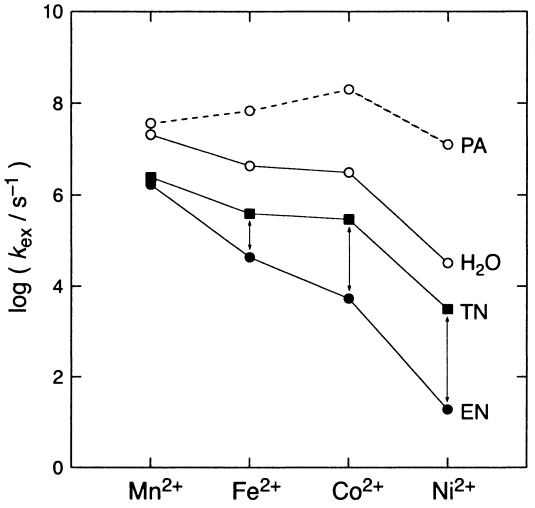

Fig. 14. Variation of $\log(k_{ex}/s^{-1})$ for the solvent exchange reactions of Mn^{2+}, Fe^{2+}, Co^{2+}, and Ni^{2+} in EN, TN, PA, and water.

Mn^{2+} to Ni^{2+}, and the k_{ex} value of Ni^{2+} in EN is substantially smaller than that in TN. According to the compilation of the crystal structures for a number of $[M(en)_3]^{m+}$ complexes,[117] the Ni–N distance (212 pm) in $[Ni(en)_3]^{2+}$ is the maximum limit to form a suitable 5-membered EN chelate, and the longer M–N bond leads to the gradual decrease of the M–N–C angle from the ideal value of ca. 109°. This means that the EN chelate complexes are destabilized with an increase in the M–N bond length due to the chelate strain in the ground state (the chelate strain effect). Thus, the 5-membered EN chelate is unfavorable for the elongation of one M–N bond in the activation process, which requires an energy greater than the corresponding 6-membered TN chelate. This difference is clearly observed in the difference in $\Delta^{\ddagger}H^{\circ}$ of Ni^{2+} between EN and TN. The smaller difference in k_{ex} for M^{2+} having the longer M–N bond length is ascribed to the destabilized ground state for the 5-membered EN chelate.

On the basis of the steric effects described above, we will consider the origin of the chelate effect. The chelate formation process for the bidentate amine ligand is expressed by two successive steps: i,e., the first coordination of one of two binding atoms to the metal ion and the following chelate ring closure, as shown in Scheme 1. The equilibrium constant (K_f) of the chelate formation reaction is given by Eq. 21:

$$K_f = \frac{k_{12}k_{23}}{k_{21}k_{32}} \tag{21}$$

Generally, the chelate effect observed as a large K_f value for the multidentate ligand compared with the corresponding value for the unidentate ligand can be partially ascribed to a large ring-closing rate, k_{23}, because of a local concentration effect. However, the k_{ex} values of TN and EN are rather small in comparison with those in PA for all metal ions given in Table 10. It

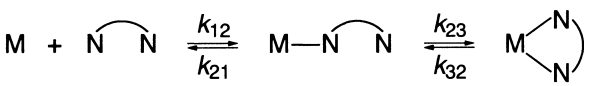

Scheme 1.

is thus strongly suggested that the larger K_f value of the bidentate ligand should be ascribed to the smaller k_{32} value. In the transition state for the chelate ring opening, the elongated M–N bond in the chelate complexes should decrease the M–N–C angle and significantly weaken the σ bonding compared to the case of complexes with unidentate ligands. The relatively large enthalpy loss for the chelate complexes in the transition state is responsible for the large activation energy for the chelate opening. This is the origin of the smaller k_{32} value, and this is the kinetic chelate effect.

As seen from Fig. 14, the k_{ex} values for all four M^{2+} ions in unidentate PA are larger than those in EN and TN, and this rate enhancement is much more pronounced for the heavier M^{2+} ion. Since the PA molecule has a very strong electron donating ability, the larger electronic repulsions occur for the heavier member. Therefore, we can expect the relatively easier PA dissociation for the heavier M^{2+} ions with the higher d orbital occupancy due to the larger d-electronic repulsions.

4. Summary

In this article, we presented a summation of the possible solvation structures of the metal ions determined by the EXAFS technique and we discussed some topical results of the solvent exchange kinetics for the metal ions studied by the NMR technique.

The solvation structures of the metal ions are affected mainly by the ionic size, ionic charge, and electronic configuration of the metal ions and by the bulkiness of the coordinating solvent molecule. An increase in the ionic radius can reduce the interligand repulsions. The increase in the ionic charge can produce a larger interaction energy between the metal ion and the coordinating solvent. In water, the hydration number varies from 4 for Be^{2+} to ca. 11 for some actinides(IV) ions according to the increase in the ionic radius and charge. Although the solvation numbers of Mn^{2+} and Ni^{2+} in a series of nitriles (AN, PN, BuN, iBuN, BzN, and VN) are 6, the steric hindrance in the first solvation sphere for the solvent exchange may be different due to the difference in bulkiness of the substituent. In the case of Ni^{2+} of which the solvent exchange proceeds via the dissociative mechanism in small AN, the solvent exchange mechanism still remains the dissociative mode of activation in bulkier nitriles. On the other hand, in the case of Mn^{2+}, in which the solvent exchange takes the associative mode in AN, the mechanism becomes less associative in response to the bulkiness of the nitrile, because the first solvation sphere of Mn^{2+} is more crowded in the bulkier nitriles during the activation process. The bulkiness effect of DMSO and DMF on the solvation number appears only for some lanthanide(III) ions (La^{3+}–Gd^{3+}), which take the hydration number of 9 or the mixture of 9 and 8, and their solvation number is reduced to 8 in DMSO and DMF. The decrease in solvation number is found in DMA and TMP, but their bulkiness is not effective for the 3d-block metal ions except for Zn^{2+} with the smaller ionic radius. In much bulkier solvents, such as TMU and HMPA, the solvation numbers of most metal ions are reduced in comparison to those in less bulky solvents. All these trends mentioned above result in the balance of both the attractive interaction between the ionic charge and the solvent dipole and the repulsive interaction between the solvent dipoles ar-

ranged around the metal center.

Interestingly, the 4-coordinate solvate of Co^{2+} exists in PA. Because the PA molecule has a strong σ-donating ability, such a low solvation number of 4 can be established by both the increase in the electronic repulsion between the 3d electrons of Co^{2+} and the decrease in the attractive interaction between Co^{2+} and the coordinating PA molecules. In TMU, whose the bulkiness is inferior to that of HMPA, a peculiar variation in the solvation structure appears for a series of 3d-block metal(II) ions, such as Co^{2+} (4-coordinate) and Ni^{2+} (5-coordinate), in response to the number of 3d electrons. These results indicate the additional contribution of the d electron configuration to the solvation structure.

The mechanisms for the solvent exchange reactions are very sensitive to the environments around the central metal ions. Since the metal ion assembles as many as possible solvent molecules to gain the maximum solvation energy in the ground state, the solvent density around the metal ion should become necessarily larger than that in the bulk phase. This leads to steric saturation in the first solvation sphere, and the electrostatic repulsions between the solvent molecules thus inhibit the associative approach of an entering solvent molecule. In fact, the solvent exchange mechanisms with the dissociative mode of activation are operative for many metal ions in various solvents. However, the associative mechanism becomes operative due to some special situations. One is the case of the reduced solvation number caused by the small ionic radius or the bulkiness of the solvent molecule. The solvent exchange reactions of the 4-coordinate smallest Be^{2+} ion in less bulky solvents and the 4-coordinate Co^{2+} ion in bulky TMU proceed via the associative mode of activation. This associative mode is attributable to weaker interligand repulsions in the transition state with the increased solvation number of 5. In addition, an additional energy gained by the interaction between the metal ion and an entering solvent molecule can effectively compensate the interligand repulsions. The second situation is in the case of the higher charge of the metal ion. The interligand repulsions between the solvent molecules are partly compensated by the larger attractive interaction between the entering solvent molecule and the metal ion with the higher positive charge. This is confirmed by comparison with the reaction mechanisms of the 3d-block M^{2+} and M^{3+} ions in water. The third situation is in the case of the larger ionic radius, i.e., the longer bond length between the metal ion and the coordinating atom. The longer distance can reduce the interligand repulsions in the transition state. However, as clearly observed for Mn^{2+} in a variety of solvents, the associative mechanism in less bulky solvents is changed to be less associative in response to the bulkiness of the entering solvent molecule.

The solvent exchange mechanism is easily changed between two limiting mechanisms (D and A mechanisms) even for a certain metal ion. There is no simple relationship between the activation free energy (rate constant) and the characteristics of the metal ion and/or the solvent molecule. It is very important to take into consideration the difference in the reaction mechanism when the reaction rates are compared. We can emphasize the usefulness of the activation volume in order to assign the mechanisms of the solvent exchange reactions. As shown in the case of Ni^{2+} in a series of nitriles, the $\Delta^{\ddagger}V^{\circ}$ values are almost constant (ca. 13 $cm^3\ mol^{-1}$) regardless of the large variation in bulkiness of the substituents, and the positive values are certainly connected to the dissociative mechanism. However, it should be noted that the connection between the $\Delta^{\ddagger}V^{\circ}$ value and the reaction mechanism should be considered on the basis of a reasonable estimation of the inner sphere.

The results discussed here for both subjects (solvation structure and solvent exchange reaction) are essential and necessary in order to understand the reactivities of the metal ions in solution. Such investigations will be continued in the future in order to clarify the interactions around the metal ion. If we can clarify the intrinsic aspects of the energetics for the interactions between the metal ions and the solvent molecules, we can propose a more realistic model for the ligand substitutions of the metal ions and can predict the thermodynamic and kinetic behaviors for the chemical reactions concerning the metal ions.

The authors sincerely thank all the co-workers and students whose names appear in the references and who devoted themselves to the present study. The financial support by the Grants-in-Aid for Scientific Research (Nos. 11354009, 11554030, and 12874094) from the Ministry of Education, Science, Sports and Culture is gratefully acknowledged.

References

1 H. Ohtaki and T. Radnai, *Chem. Rev.*, **93**, 1157 (1993).

2 M. Magini, G. Licheri, G. Paschina, G. Piccaluga, and G. Pinna, "X-ray Diffraction of Ions in Aqueous Solutions: Hydration and Complex Formation," CRC Press, Florida (1988).

3 C. H. Langford and H. B. Gray, "Ligand Substitution Processes," Benjamin, New York (1966).

4 S. Funahashi, in "High Pressure Liquids and Solutions," ed by Y. Taniguchi, M. Senoo, and K. Hara, Elsevier, Amsterdam (1994), pp. 33-48.

5 P. A. Lee, P. H. Citrin, P. Eisenberger, and B. M. Kincaid, *Rev. Mod. Phys.*, **53**, 769 (1981).

6 Y. Marcus, *Chem. Rev.*, **88**, 1475 (1988).

7 J. A. Victoreen, *J. Appl. Phys.*, **19**, 855 (1948).

8 W. H. McMaster, N. Kerr, D. Grande, J. H. Mallet, and J. H. Hubell, "Compilation of X-ray Cross Sections," National Technical Information Service, Springfield (1969).

9 F. J. Harris, *Proc. IEEE*, **66**, 51 (1978).

10 J. J. Rehr and R. C. Albers, *Rev. Mod. Phys.*, **72**, 621 (2000).

11 S. I. Zabinsky, J. J. Rehr, A. Ankudinov, R. C. Albers, and M. J. Eller, *Phys. Rev. B*, **52**, 2995 (1995).

12 M. Newville, R. Ravel, D. Haskel, J. J. Rehr, E. A. Stern, and Y. Yacoby, *Phys. B*, **208/209**, 154 (1995).

13 T. Teranishi, M. Harada, K. Asakura, H. Asanuma, Y. Saito, and N. Toshima, *J. Chem. Phys.*, **98**, 7967 (1994).

14 Y. Inada, H. Hayashi, K. Sugimoto, and S. Funahashi, *J. Phys. Chem. A*, **103**, 1401 (1999).

15 P. Lindqvist-Reis, J. Näslund, I. Persson, and M. Sandström, *J. Chem. Soc., Dalton Trans.*, **2000**, 2703.

16 Y. Tsutsui, K. Sugimoto, H. Wasada, Y. Inada, and S. Funahashi, *J. Phys. Chem. A*, **101**, 2900 (1997).

17 K. Ozutsumi, T. Takamuku, S. Ishiguro, and H. Ohtaki, *Bull. Chem. Soc. Jpn.*, **65**, 2104 (1992).

18 S. Funahashi and Y. Inada, *Trends Inorg. Chem.*, **5**, 15

(1998).
19 J. Näslund, I. Persson, and M. Sandström, *Inorg. Chem.*, **39**, 4012 (2000).
20 B. Hellquist, L. A. Bengtsson, B. Holmberg, B. Hedman, I. Persson, and L. I. Elding, *Acta Chem. Scand.*, **45**, 449 (1991).
21 K. Ozutsumi, M. Koide, H. Suzuki, and S. Ishiguro, *J. Phys. Chem.*, **97**, 500 (1993).
22 S. Ishiguro, Y. Umebayashi, K. Kato, R. Takahashi, and K. Ozutsumi, *J. Chem. Soc., Faraday Trans.*, **94**, 3607 (1998).
23 T. Yamaguchi, M. Nomura, H. Wakita, and H. Ohtaki, *J. Chem. Phys.*, **89**, 5153 (1988).
24 Y. Inada, N. Nakayama, S. Okayama, and S. Funahashi, unpublished results.
25 R. D. Shannon, *Acta Crystallogr. A*, **32**, 751 (1976).
26 Y. Inada, K. Sugimoto, K. Ozutsumi, and S. Funahashi, *Inorg. Chem.*, **33**, 1875 (1994).
27 K. Ozutsumi, Y. Abe, R. Takahashi, and S. Ishiguro, *J. Phys. Chem.*, **98**, 9894 (1994).
28 Y. Abe, R. Takahashi, S. Ishiguro, K. Ozutsumi, *J. Chem. Soc., Dalton Trans.*, **88**, 1997 (1992).
29 S. F. Lincoln and A. White, *Inorg. Chim. Acta*, **168**, 265 (1990).
30 A. B. P. Lever, "Inorganic Electronic Spectroscopy," 2nd ed., Elsevier, Amsterdam (1984).
31 J. T. Donoghue and R. S. Drago, *Inorg. Chem.*, **2**, 1158 (1963).
32 Y. Inada, Y. Itoh, H. Kuwabara, and S. Funahashi, *Inorg. Reac. Mech.*, **2**, 161 (2000).
33 Y. Inada, N. Hotta, H. Kuwabara, and S. Funahashi, *Anal. Sci.*, **17**, 187 (2001).
34 Y. Inada, K. Sugimoto, K. Ozutsumi, and S. Funahashi, *Inorg. Chem.*, **37**, 1886 (1998).
35 Y. Inada and S. Funahashi, *Anal. Sci.*, **13**, 373 (1997).
36 Y. Inada, Y. Tsutsui, H. Wasada, and S. Funahashi, *Z. Naturforsch. B*, **54**, 193 (1999).
37 L. M. Engelhardt, C. Pakawatchai, and A. H. White, *J. Chem. Soc., Dalton Trans.*, **1985**, 117.
38 M. Kurihara, K. Ozutsumi, and T. Kawashima, *J. Solution. Chem.*, **24**, 719 (1995).
39 S. Aizawa, S. Iida, K. Matsuda, and S. Funahashi, *Inorg. Chem.*, **35**, 1338 (1996).
40 I. Persson, J. E. Penner-Hahn, and K. O. Hodgson, *Inorg. Chem.*, **32**, 2497 (1993).
41 T. Yamaguchi, H. Wakita, and M. Nomura, *J. Chem. Soc., Chem. Commun.*, **1988**, 433.
42 S. Ahrland, K. Nilsson, I. Persson, A. Yuchi, and J. E. Penner-Hahn, *Inorg. Chem.*, **28**, 1833 (1989).
43 S. F. Frisch, G. W. Trucks, M. Head-Gordon, P. M. W. Gill, M. W. Wong, J. B. Foresman, B. G. Johnson, H. B. Schlegel, M. A. Robb, E. S. Replogle, R. Gomperts, J. L. Andres, K. Raghavachari, J. S. Binkley, C. Gonzalez, R. L. Martin, D. J. Fox, D. J. Defrees, J. Baker, J. J. P. Stewart, and J. A. Pople, "Gaussian 92 Revision C," Gaussian Inc., Pittsburgh PA (1992).
44 M. J. Frisch, G. W. Trucks, H. B. Schlegel, G. E. Scuseria, M. A. Robb, J. R. Cheese-man, V. G. Zakrewski, J. A. Montgomery, R. E. Stratmann, J. C. Burant, S. Dapprich, J. M. Millam, A. D. Daniels, K. N. Kudin, M. C. Strain, O. Farkas, J. Tomasi, V. Barone, M. Cossi, R. Cammi, B. Mennucci, C. Pomelli, C. Adamo, S. Clifford, J. Ochterski, G. A. Petersson, P. Y. Ayala, Q. Cui, K. Morokuma, D. K. Malick, A. D. Rabuck, K. Raghavachari, J. B. Foresman, J. Cioslowski, J. V. Ortiz, B. B. Stefanov, G. Liu, A. Liashenko, P. Piskorz, I. Komaromi, R. Gomperts, R. L. Martin, D. J. Fox, T. Keith, M. A. Al-Laham, C. Y. Peng, A. Nanayakkara, C. Gonzalez, M. Challacombe, P. M. W. Gill, B. G. Johnson, W. Chen, M. W. Wong, J. L. Andres, M. Head-Gordon, E. S. Replogle, and J. A. Pople, "Gaussian 98 Revision A. 7," Gaussian Inc., Pittsburgh PA (1998).
45 S. F. Boys and F. Bernardi, *Mol. Phys.*, **19**, 553 (1970).
46 H. A. C. McKay, *J. Am. Chem. Soc.*, **65**, 702 (1943).
47 H. M. McConnell, *J. Chem. Phys.*, **28**, 430 (1958).
48 I. Bertini and C. Luchinat, "NMR of Paramagnetic Molecules in Biological Systems," Benjamin, California (1986).
49 J. Mason, "Multinuclear NMR," Plenum Press, New York (1987).
50 J. R. Zimmermann and W. E. Brittin, *J. Phys. Chem.*, **61**, 1328 (1957).
51 T. J. Swift and R. E. Connick, *J. Chem. Phys.*, **37**, 307 (1962).
52 Z. Luz and S. Meiboom, *J. Chem. Phys.*, **40**, 2686 (1964).
53 M. Ishii, S. Funahashi, and M. Tanaka, *Inorg. Chem.*, **27**, 3192 (1988).
54 M. Ishii, S. Funahashi, K. Ishihara, and M. Tanaka, *Bull. Chem. Soc. Jpn.*, **62**, 1852 (1989).
55 I. Solomon, *Phys. Rev.*, **99**, 559 (1955).
56 N. Bloembergen, *J. Chem. Phys.*, **27**, 575 (1957).
57 N. Bloembergen and L. O. Morgan, *J. Chem. Phys.*, **34**, 842 (1961).
58 M. Rubinstein, A. Baram, and Z. Luz, *Mol. Phys.*, **20**, 67 (1971).
59 H. M. McConnell and D. B. Chesnut, *J. Chem. Phys.*, **28**, 107 (1958).
60 J. P. Jesson, *J. Chem. Phys.*, **47**, 579, 582 (1967).
61 R. J. Kurland and B. R. McGarvey, *J. Magn. Reson.*, **2**, 286 (1970).
62 R. M. Nielson, H. W. Dodgen, J. P. Hunt, and S. E. Wherland, *Inorg. Chem.*, **25**, 582 (1986).
63 L. L. Rusnak and R. B. Jordan, *Inorg. Chem.*, **15**, 709 (1976).
64 H. G. Hertz, *Z. Electrochem.*, **65**, 20 (1961).
65 S. F. Lincoln and A. E. Merbach, *Adv. Inorg. Chem.*, **42**, 1 (1995).
66 D. Hugi-Cleary, L. Helm, and A. E. Merbach, *Helv. Chim. Acta*, **68**, 545 (1985).
67 D. Hugi-Cleary, L. Helm, and A. E. Merbach, *J. Am. Chem. Soc.*, **109**, 4444 (1987).
68 P.-A. Pittet, G. Elbaze, L. Helm, and A. E. Merbach, *Inorg. Chem.*, **29**, 1936 (1990).
69 L. Helm, L. I. Elding, and A. E. Merbach, *Helv. Chim. Acta*, **67**, 1453 (1984).
70 L. Helm, L. I. Elding, and A. E. Merbach, *Inorg. Chem.*, **24**, 1719 (1985).
71 A. D. Hugi, L. Helm, and A. E. Merbach, *Inorg. Chem.*, **26**, 1763 (1987).
72 A. D. Hugi, L. Helm, and A. E. Merbach, *Helv. Chim. Acta*, **68**, 508 (1985).
73 M. Grant and R. B. Jordan, *Inorg. Chem.*, **20**, 55 (1981).
74 T. W. Swaddle and A. E. Merbach, *Inorg. Chem.*, **20**, 4212 (1981).
75 I. Rapaport, L. Helm, A. E. Merbach, P. Bernhard, and A. Ludi, *Inorg. Chem.*, **27**, 873 (1988).
76 G. Laurenczy, I. Rapaport, D. Zbinden, and A. E. Merbach, *Magn. Reson. Chem.*, **29**, S45 (1991).

77 C. Cossy, L. Helm, and A. E. Merbach, *Inorg. Chem.*, **28**, 2699 (1989).
78 A. Cusanelli, U. Frey, D. T. Richens, and A. E. Merbach, *J. Am. Chem, Soc.*, **118**, 5265 (1996).
79 Y. Ducommun, D. Zbinden, and A. E. Merbach, *Helv. Chim. Acta*, **65**, 1385 (1982).
80 Y. Ducommun, K. E. Newman, and A. E. Merbach, *Inorg, Chem.*, **19**, 3696 (1980).
81 D. H. Powell, L. Helm, and A. E. Merbach, *J. Chem. Phys.*, **95**, 9258 (1991).
82 D. H. Powell, P. Furrer, P.-A. Pittet, and A. E. Merbach, *J. Phys. Chem.*, **99**, 16622 (1995).
83 S.-K. Kang, B. Lam, T. A. Albright, and J. F. O'Brien, *New. J. Chem.*, **15**, 757 (1991).
84 R. Åkesson, L. G. M. Pettersson, M. Sandström, P. E. M. Siegbahn, and U. Wahlgren, *J. Phys. Chem.*, **97**, 3765 (1993).
85 R. Åkesson, L. G. M. Pettersson, M. Sandström, and U. Wahlgren, *J. Am. Chem. Soc.*, **116**, 8705 (1994).
86 F. P. Rotzinger, *J. Am. Chem. Soc.*, **118**, 6760 (1996).
87 F. P. Rotzinger, *J. Am. Chem. Soc.*, **119**, 5230 (1997).
88 M. Hartmann, T. Clark, and R. van Eldik, *J. Am. Chem. Soc.*, **119**, 7843 (1997).
89 R. J. Deeth and L. L. Elding, *Inorg. Chem.*, **35**, 5019 (1996).
90 Y. Tsutsui, H. Wasada, and S. Funahashi, *Bull. Chem. Soc. Jpn.*, **70**, 1813 (1997).
91 Y. Tsutsui, H. Wasada, and S. Funahashi, *Bull, Chem. Soc. Jpn.*, **71**, 73 (1998).
92 Y. Tsutsui, H. Wasada, and S. Funahashi, *Bull. Chem. Soc. Jpn.*, **71**, 1771 (1998).
93 Y. Tsutsui, H. Wasada, and S. Funahashi, *J. Mol. Struct. (Theochem)*, **461-462**, 379 (1999).
94 R. van Eldik, W. Gaede, H. Cohen, and D. Meyerstein, *Inorg. Chem.*, **31**, 3695 (1992).
95 F. Fittipaldi and S. Petrucci, *J. Phys. Chem.*, **71**, 3414 (1967).
96 D. de Vito, H. Sidorenkova, F. P. Rotzinger, J. Weber, and A. E. Merbach, *Inorg. Chem.*, **39**, 5547 (2000).
97 Y. Inada, A. M. Mohammed, H. H. Loeffler, and B. M. Rode, *J. Phys. Chem. A*, in press.
98 V. Gutmann, "The Donor-Acceptor Approach to Molecular Interactions," Plenum Press, New York (1978).
99 S. G. Lias, J. F. Liebman, and R. D. Levin, *J. Phys. Chem. Ref. Data*, **13**, 695 (1984).
100 J. A. Riddick, W. B. Bunger, and T. K. Sakano, "Organic Solvents," 4th ed, John Wiley & Sons, New York (1986).
101 T. Radnai, S. Itoh, and H. Ohtaki, *Bull. Chem. Soc. Jpn.*, **61**, 3845 (1988).
102 M. Ishii, S. Funahashi, and M. Tanaka, *Chem. Lett.*, **1987**, 871.
103 A. Hioki, S. Funahashi, M. Ishii, and M. Tanaka, *Inorg. Chem.*, **25**, 1360 (1986).
104 F. K. Meyer, K. E. Newman, and A. E. Merbach, *J. Am. Chem. Soc.*, **101**, 5588 (1979).
105 J.-C. Boubel and J.-J. Delpuech, *Adv. Mol. Relax. Processes*, **7**, 209 (1975).
106 C. Cossy, L. Helm, and A. E. Merbach, *Helv. Chim. Acta*, **70**, 1516 (1987).
107 T.-M. Chen and L. O. Morgan, *J. Phys. Chem.*, **76**, 1973 (1972).
108 Y. Marcus, "Ion Solvation," John Wiley & Sons, Chichester (1985).
109 F. K. Meyer, K. E. Newman, and A. E. Merbach, *Inorg. Chem.*, **18**, 2142 (1979).
110 C. H. McAteer and P. Moore, *J. Chem. Soc., Dalton Trans.*, **1983**, 353.
111 N. A. Matwiyoff, *Inorg. Chem.*, **5**, 788 (1966).
112 J.-J. Delpuech, M. R. Khaddar, A. A. Peguy, and P. R. Rubini, *J. Am. Chem. Soc.*, **97**, 3377 (1975).
113 K. Micskei, D. H. Powell, L. Helm, E. Brücher, and A. E. Merbach, *Magn. Reson. Chem.*, **31**, 1011 (1993).
114 D. L. Pisaniello, L. Helm, P. Meier, and A. E. Merbach, *J. Am. Chem. Soc.*, **105**, 4528 (1983).
115 S. Soyama, M. Ishii, S. Funahashi, and M. Tanaka, *Inorg. Chem.*, **31**, 536 (1992).
116 Y. Inada, K. Ozutsumi, S. Funahashi, S. Soyama, T. Kawashima, and M. Tanaka, *Inorg. Chem.*, **32**, 3010 (1993).
117 S. Aizawa, K. Matsuda, T. Tajima, M. Maeda, T. Sugata, and S. Funahashi, *Inorg. Chem.*, **34**, 2042 (1995).
118 S. Aizawa, S. Iida, K. Matsuda, and S. Funahashi, *Bull. Chem. Soc. Jpn.*, **70**, 1593 (1997).
119 F. Jalilehvand, D. Spångberg, P. Lindqvist-Reis, K. Hermansson, I. Persson, and M. Sandstöm, *J. Am. Chem. Soc.*, **123**, 431 (2001).
120 A. Muñoz-Páez, R. R. Pappalardo, and E. Sánchez Marcos, *J. Am. Chem. Soc.*, **117**, 11710 (1995).
121 Y. Inada and S. Funahashi, *Z. Naturforsch. B*, **54**, 1517 (1999).
122 S. Díaz-Moreno, A. Muñoz-Páez, and J. Chaboy, *J. Phys. Chem. A*, **104**, 1278 (2000).
123 J. Näslund, P. Lindqvist-Reis, I. Persson, and M. Sandström, *Inorg. Chem.*, **39**, 4006 (2000).
124 G. Ma, A. Molla-Abbassi, M. Kritikos, A. Ilyukhin, F. Jalilehvand, V. Kessler, M. Skripkin, M. Sandstöm, J. Glaser, J. Näslund, and I. Persson, *Inorg. Chem.*, **40**, 6432 (2001).
125 H. Moll, M. A. Denecke, F. Jalilehvand, M. Sandström, and I. Grenthe, *Inorg. Chem.*, **38**, 1795 (1999).
126 P. G. Allen, J. J. Bucher, D. K. Shuh, N. M. Edelstein, T. Reich, *Inorg. Chem.*, **36**, 4676 (1997).
127 M. Inamo, N. Kamiya, Y. Inada, M. Nomura, and S. Funahashi, *Inorg. Chem.*, **40**, 5636 (2001).
128 Y. Inada, K. Sugimoto, Y. Nakano, Y. Itoh, and S. Funahashi, *Inorg. Chem.*, **37**, 5519 (1998).
129 M. Valli, S. Matsuo, H. Wakita, T. Yamaguchi, and M. Nomura, *Inorg. Chem.*, **35**, 5642 (1996).
130 F.-C. Xu, H. R. Krouse, and T. W. Swaddle, *Inorg. Chem.*, **24**, 267 (1985).
131 G. E. Glass, W. B. Schwabacher, and R. S. Tobias, *Inorg. Chem.*, **7**, 2471 (1968).
132 F. W. Breivogel, *J. Chem. Phys.*, **51**, 445 (1969).

Shigenobu Funahashi was born in Aichi in 1941. He graduated from the Department of Chemistry, Faculty of Science, Nagoya University, in 1965, and received his M.S. degree (1967) and D.S. degree (1971) from the same university. He became Research Associate at Nagoya University in 1970 and was appointed as Associate Professor in 1973. He left to work as a postdoctoral fellow with Professor Robert B. Jordan at Alberta University for a year in 1973–1974. He was promoted to Professor at Graduate School of Science, Nagoya University, in 1990. His research is concerned with dynamic aspects in analytical chemistry, dynamic behaviors of metal ions in solution, and structural aspects of short-lived intermediates. He received the Japan Society for Analytical Chemistry Award, 2000.

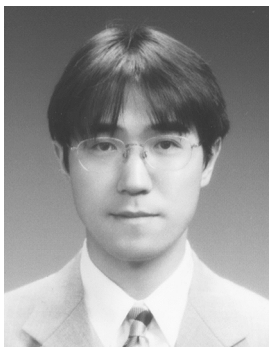

Yasuhiro Inada was born in Fukui in 1967. He graduated from the Department of Chemistry, Faculty of Science, Nagoya University, in 1990, and received his M.S. degree (1992) and D.S. degree (1998) from the same university. He obtained a position as Research Associate at Nagoya University in 1992. He studied as a postdoctoral fellow with Professor Bernd M. Rode at the University of Innsbruck for a year in 2000–2001. His research interests include kinetic evaluations of fast inorganic reactions in solution, developments of time-resolved EXAFS instruments, and quantum-mechanical molecular dynamic simulations of metal ions. He received the Japan Society for Analytical Chemistry Award for Younger Researchers, 1999.